Bacteriophage protein Dap1 regulates evasion of antiphage immunity and *Pseudomonas aeruginosa* virulence impacting phage therapy in mice

Check for updates

Shuai Le [1,2,8], Leilei Wei[3,4,8], Jing Wang[1,2,8], Fang Tian[4], Qian Yang[5], Jingru Zhao[5], Zhuojun Zhong[1,2], Jiazhen Liu[1,2], Xuesong He [6], Qiu Zhong[3], Shuguang Lu[1,2] & Haihua Liang [4,7] ✉

Bacteriophages have evolved diverse strategies to overcome host defence mechanisms and to redirect host metabolism to ensure successful propagation. Here we identify a phage protein named Dap1 from *Pseudomonas aeruginosa* phage PaoP5 that both modulates bacterial host behaviour and contributes to phage fitness. We show that expression of Dap1 in *P. aeruginosa* reduces bacterial motility and promotes biofilm formation through interference with DipA, a c-di-GMP phosphodiesterase, which causes an increase in c-di-GMP levels that trigger phenotypic changes. Results also show that deletion of *dap1* in PaoP5 significantly reduces genome packaging. In this case, Dap1 directly binds to phage HNH endonuclease, prohibiting host Lon-mediated HNH degradation and promoting phage genome packaging. Moreover, PaoP5Δ*dap1* fails to rescue *P. aeruginosa*-infected mice, implying the significance of *dap1* in phage therapy. Overall, these results highlight remarkable dual functionality in a phage protein, enabling the modulation of host behaviours and ensuring phage fitness.

The arms race between bacteria and bacteriophages (phages) has led to the evolution of diverse antiphage elements[1–3], such as CRISPR-Cas systems and restriction-modification systems (RM)[4]. Phages usually rely on diverse counterstrategies to evade these antiviral systems[5,6], including anti-CRISPR proteins[7] and anti-restriction endonuclease proteins[8]. Moreover, the prokaryotic antiphage defence mechanisms are much more complex than previously perceived, and many prokaryotic defence systems and antidefence mechanisms are still unknown[9]. Thus, studies on phage and bacterial genes may reveal numerous biological mechanisms involved in phage–host interactions.

Phage-resistance genes are diverse, comprising nucleases, helicases, proteases and kinases[10]. The nucleases from the RM and CRISPR-Cas systems that cleave phage DNA have been investigated extensively[11]. In contrast, the role of proteases in phage defence is poorly studied. Proteases are commonly identified in phage defence systems[12–16]. However, whether these proteases directly cleave phage protein to defend against phage infection is yet to be determined.

[1]Department of Microbiology, College of Basic Medical Sciences, Key Laboratory of Microbial Engineering Under the Educational Committee in Chongqing, Army Medical University, Chongqing, China. [2]State Key Laboratory of Trauma and Chemical Poisoning, Chongqing, China. [3]Department of Laboratory Medicine, Daping Hospital, Army Medical University, Chongqing, China. [4]College of Medicine, Southern University of Science and Technology, Shenzhen, China. [5]College of Life Sciences, Northwest University, Xi'an, China. [6]The ADA Forsyth Institute, Cambridge, MA, USA. [7]University Laboratory of Metabolism and Health of Guangdong, Southern University of Science and Technology, Shenzhen, China. [8]These authors contributed equally: Shuai Le, Leilei Wei, Jing Wang. ✉e-mail: lianghh@sustech.edu.cn

On the other hand, given that phages strictly rely on the host cell for propagation, they have evolved different strategies to redirect the bacterial metabolism to establish an efficient infection cycle[17,18], such as interfering with RNA transcription, DNA replication, protein translation and cell division pathways in bacteria[19]. The phage proteins that could manipulate host behaviour are mainly expressed in the early stages of infection, and studies of phage-inspired antibacterial strategies could provide new targets for developing antimicrobial drugs[18,20].

Tens of thousands of complete phage genomes have been sequenced, and over two-thirds of phage genes are functionally unknown, many of which could potentially encode important functions to manipulate the host and overcome bacterial defence mechanisms[21–24]. *Pseudomonas aeruginosa* phage PaoP5 has a linear double-stranded DNA (dsDNA) genome with 176 predicted protein-encoding genes, while the function of over 80.7% of these open reading frames (ORFs) is uncharacterized. Interestingly, many of these hypothetical proteins are relatively conserved and share over 90% identity with the corresponding genes in other PAK_P1-like *P. aeruginosa* phages isolated from Asia, Europe and Africa[25]. This finding suggests that these genes might be essential for phage survival under specific conditions and some of them may encode antidefence mechanisms or host-takeover strategies.

In this study, we tried to systematically study the function of hypothetical proteins in *P. aeruginosa* phage PaoP5 and identified a dual-functional phage protein that simultaneously regulates bacterial virulence and protects phage from bacterial defence.

Results

Phage protein Dap1 inhibits bacterial motility

We tried to identify genes in phage PaoP5, which has a relatively broad host range (Extended Data Fig. 1a), that inhibit bacterial motility but do not affect bacterial growth (Fig. 1a), as bacterial motility and biofilm are important virulent factors for *P. aeruginosa*[26–28]. Thus, we investigated the biological activities of 60 hypothetical *orfs* from PaoP5 (Supplementary Tables 1 and 2). The expression of *orf002, orf157, orf160, orf163, orf164, orf165* or *orf176* in PAO1 triggered a striking growth defect (Extended Data Fig. 1b), indicating that these gene products are potentially toxic to *P. aeruginosa*. Interestingly, among the other 53 non-toxic genes, overexpression of *orf003* (hereafter referred to as Dap1, Defence antiphage protein 1) significantly inhibited bacterial swimming and swarming (Fig. 1b) without affecting bacterial growth (Extended Data Fig. 1b), indicating the target of Dap1 should be a bacterial motility-associated protein.

RNA sequencing (RNA-seq) was used to gain insight into how Dap1 affects bacterial motility. Expression of *dap1* led to differential regulation of 166 genes during exponential growth. Among these, 52 genes were upregulated and 114 genes were downregulated in the PAO1/*p-dap1* strain (DEGs) (>2-fold change and $P < 0.05$) (Fig. 1c). The most enriched Kyoto Encyclopedia of Genes and Genomes (KEGG) pathways of the differentially expressed genes (DEGs) are phenazine biosynthesis, quorum sensing and biofilm formation (Extended Data Fig. 2a,b and Supplementary Table 1). In addition, the reliability of the RNA-seq data was validated by quantitative PCR with reverse transcription (RT–qPCR) (Extended Data Fig. 2c).

Dap1 interacts with DipA to regulate host behaviours

Notably, RNA-seq data showed that *siaC* and *siaD*, which are required for biofilm formation[29], were significantly upregulated in PAO1/*p-dap1* strain (Supplementary Table 1). Thus, we next investigated whether Dap1 affects *P. aeruginosa* biofilm formation. Our data revealed that biofilm formation of *P. aeruginosa* expressing *dap1* is in an isopropyl-β-D-thiogalactopyranoside (IPTG) dose-dependent manner, while IPTG did not affect biofilm formation of PAO1 carrying vector control (Extended Data Fig. 3a). A COMSTAT analysis also showed that the PAO1/*p-dap1* strain significantly increased biofilm biomass compared with PAO1 expressing the empty vector (Fig. 1d). These data indicate that Dap1 is able to regulate bacterial virulence. As bacterial motility and biofilm formation are inversely regulated by the second messenger signalling molecule cyclic-di-GMP (c-di-GMP)[30], we hypothesized that Dap1 controls these two phenotypes by regulating the intracellular c-di-GMP levels via its binding to diguanylate cyclase (DGC) or phosphodiesterase (PDE). To test this hypothesis, we used a bacterial adenylate cyclase two-hybrid (BACTH) assay to detect potential protein-binding partner(s) for Dap1 (Supplementary Tables 1 and 2, and Extended Data Fig. 3b). We found that the expression of DipA, RocR or ProE in combination with Dap1 resulted in a high level of β-galactosidase activity (Fig. 1e and Extended Data Fig. 4a). We further validated the interactions using co-immunoprecipitation (CO-IP) assay and found that Dap1 only co-eluted with DipA (PA5017) (Fig. 1f) but not with RocR (PA3947) or ProE (PA5295) (Extended Data Fig. 4b,c), indicating that the altered bacterial behaviours resulting from Dap1 expression are mediated through its interaction with DipA.

DipA is a c-di-GMP phosphodiesterase. The inactivation of *dipA* causes an increase in the cellular c-di-GMP level and inhibits flagellum motor switching and swimming[31]. Similar to the expression of *dap1* in PAO1, biofilm formation was enhanced while bacterial swimming and swarming motility was decreased in the Δ*dipA* mutant compared with the wild-type parent strain (Fig. 1c and Extended Data Fig. 4d). Given that Dap1 interacts with DipA, we reasoned that the expression of *dap1* in *P. aeruginosa* should alter the intracellular c-di-GMP levels. To this end, c-di-GMP levels were measured in PAO1/*p-dap1* and PAO1 harbouring the empty vector using the *p-cdrA-lux* reporter fusion, which is responsive to intracellular levels of c-di-GMP in *P. aeruginosa*[32]. Expression of *dap1* in PAO1 exhibited significantly higher levels of c-di-GMP compared with the PAO1 expressing the empty vector (Extended Data Fig. 5a), which is consistent with western-blot analysis showing that the protein production of CdrA was much higher in PAO1/*p-dap1* than in the PAO1/pME control strain (Extended Data Fig. 5b). The result was further validated using liquid chromatography mass spectrometry (LC–MS) (Fig. 1g). As expected, the expression of *dap1* did not alter

Fig. 1 | Phage protein Dap1 regulates *P. aeruginosa* virulence by interacting with c-di-GMP phosphodiesterase DipA. a, Schematic of the experimental procedure used to identify the phage genes that regulate *P. aeruginosa* motility. The early-expressed phage genes were individually cloned into the inducible plasmid pME6032 and transformed into PAO1. Subsequently, the bacterial growth and motility for each constructed strain were observed under conditions supplemented with 0.05 mM IPTG. **b**, Representative swimming and swarming plates of the indicated strains. **c**, Volcano plot of the DEGs between PAO1/*pME* and PAO1/*p-dap1* strains analysed by RNA-seq. Green dots and orange dots represent upregulated and downregulated genes, respectively, in PAO1/*p-dap1* compared with the PAO1/*pME* control. *P* values were assessed by two-sided Fisher's exact test and adjusted for multiple hypothesis testing using the Benjamini–Hochberg correction; genes with $P < 0.05$ were considered statistically significant. **d**, Representative fluorescence confocal microscope images of 36 h biofilms of *P. aeruginosa* PAO1/*pME* and PAO1/*p-dap1*. The biomass of the strains was measured in $\mu m^3 \mu m^{-2}$.
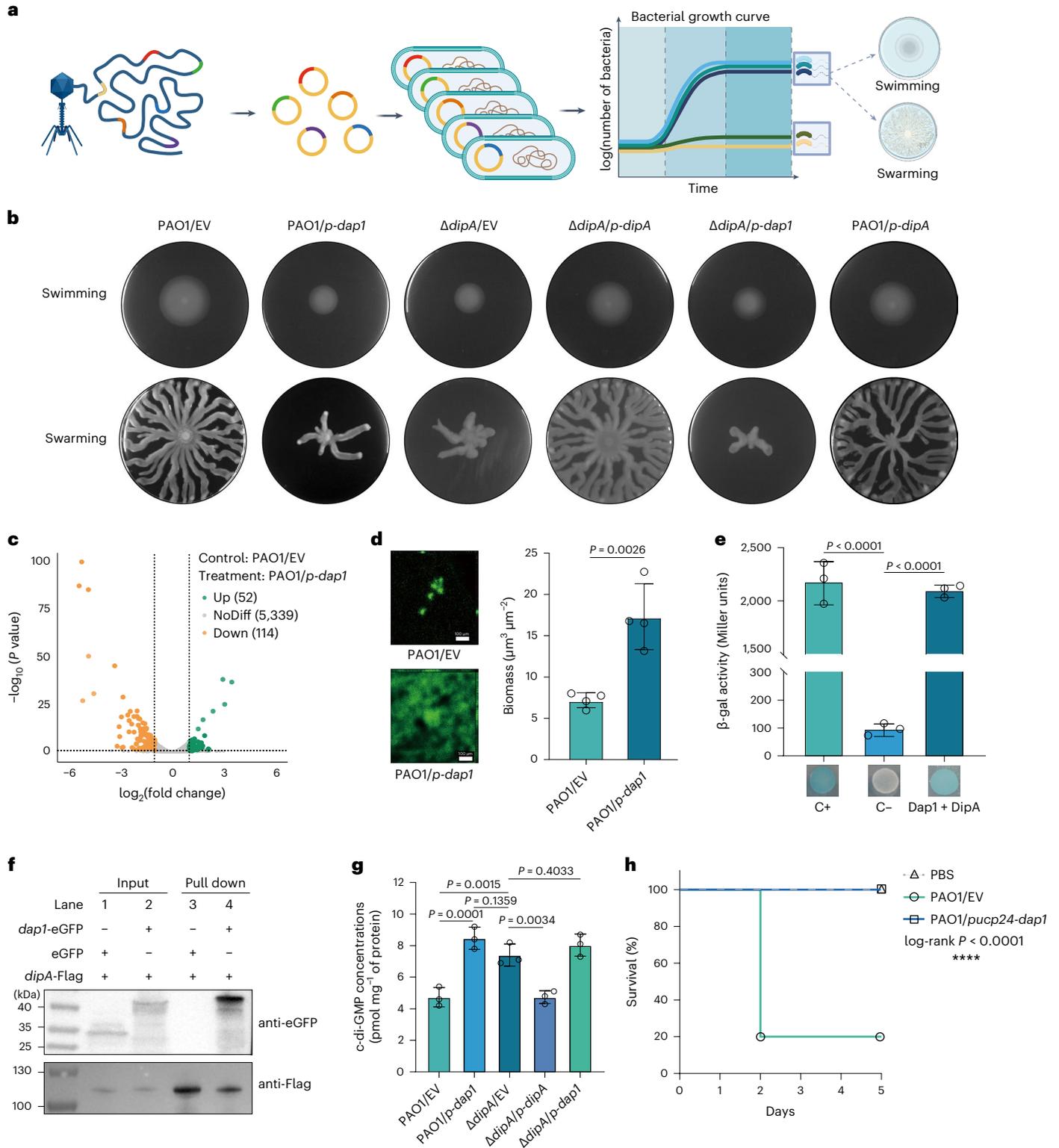
e, The bacterial two-hybrid assay indicates that Dap1 interacts with DipA. Interactions were visualized by a drop test on LB agar plates supplemented with X-gal and quantified by measuring the β-galactosidase activity, which is indicated in Miller units. C+ and C− represent the positive and negative controls, respectively. **f**, Co-IP of eGFP or *dap1*-eGFP with *dipA*-Flag. Either *dipA*-Flag and eGFP or *dipA*-Flag and *dap1*-eGFP were co-expressed in *E. coli*, and the initial samples (input) and retained proteins (pull-down) were analysed by western blot against eGFP or Flag antibody. Data are representative of 3 independent replications. **g**, Quantification of intracellular c-di-GMP levels in the indicated strains by LC–MS. **h**, Expression of *dap1* reduced the virulence of *P. aeruginosa*. 7-week-old BABL/c female mice were intranasally challenged with PAO1/pUCP24 (vector control) or PAO1/pUCP-dap1 at 2×10^7 c.f.u.s in 100 μl of PBS, and moribund mice were euthanized for survival data. Data represent mean ± s.d. (**d**, *n* = 4; **e** and **g**, *n* = 3; **h**, *n* = 5; **d**, two-sided Student's *t*-test; **e** and **g**, one-way analysis of variance (ANOVA) with Dunnett's multiple comparisons test; **h**, Kaplan–Meier (log-rank test).

the intracellular c-di-GMP levels and bacterial behaviours of the Δ*dipA* strain (Fig. 1b and Extended Data Fig. 4d).

The inhibited bacterial motility in the PAO1/*p-dap1* strain led us to investigate the role of phage Dap1 protein in PAO1 pathogenesis using a well-established mouse model of acute infection. Survival studies showed that 80% of PAO1/*pUCP*-infected mice died within 2 days, while all the PAO1/*pUCP*-dap1-infected mice demonstrated 100% survival by day 5 (Fig. 1h). Collectively, these data suggest that expression of the phage protein Dap1 inhibits the pathogenicity of *P. aeruginosa*.

Knockout of *dap1* impairs the fitness of phage

We then investigated the potential role of Dap1 in phage fitness. First, we used RT–qPCR to confirm that *dap1* is an early-expressed gene (Extended Data Fig. 6a). Next, the *dap1* gene in PaoP5 was deleted using the CRISPR-Cas9 system and knockout of *orf014* and *orf153* served as controls. Interestingly, PaoP5Δ*dap1* formed tiny plaques, while PaoP5Δ*orf14* and PaoP5Δ*orf153* formed large plaques similar to the wild-type (WT) phage (Fig. 2a). Moreover, the expression of *dap1* in PAO1 could restore the large plaques of PaoP5Δ*dap1*, while the efficiency of
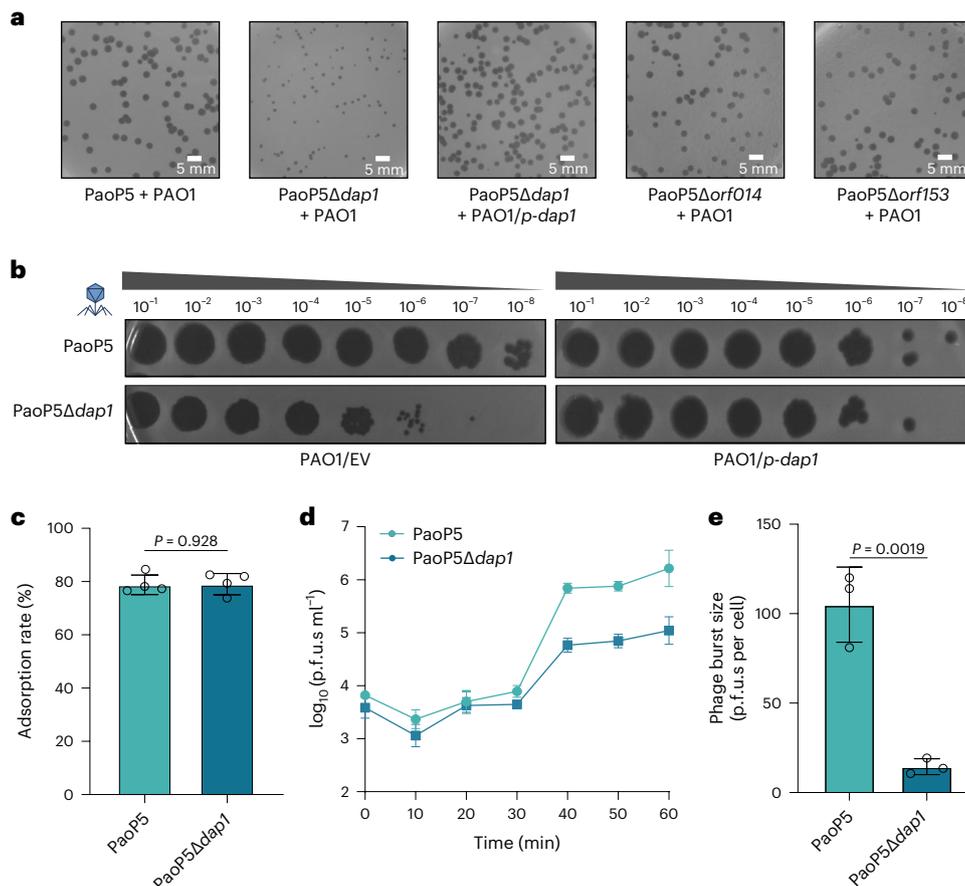

a

b

| PAO1/EV | PAO1/*p-dap1* | Δ*dipA*/EV | Δ*dipA*/*p-dipA* | Δ*dipA*/*p-dap1* | PAO1/*p-dipA* |

Swimming

Swarming

c Control: PAO1/EV
Treatment: PAO1/*p-dap1*
- Up (52)
- NoDiff (5,339)
- Down (114)

d PAO1/EV   PAO1/*p-dap1* $P = 0.0026$

e $P < 0.0001$ $P < 0.0001$ C+   C−   Dap1 + DipA

f

Lane	Input		Pull down	
	1	2	3	4
dap1-eGFP	−	+	−	+
eGFP	+	−	+	−
dipA-Flag	+	+	+	+

anti-eGFP

anti-Flag

g $P = 0.0015$ $P = 0.4033$ $P = 0.1359$ $P = 0.0001$ $P = 0.0034$

PAO1/EV, PAO1/*p-dap1*, Δ*dipA*/EV, Δ*dipA*/*p-dipA*, Δ*dipA*/*p-dap1*

h
- △ PBS
- ○ PAO1/EV
- □ PAO1/*pucp24-dap1*

log-rank $P < 0.0001$
****

Fig. 2 | PaoP5Δ*dap1* forms small plaques and produces fewer progenies.
a, PaoP5Δ*dap1* forms small phage plaques but PaoP5Δ*orf014* and PaoP5Δ*orf153* as controls show similar phage plaques as wild-type PaoP5. Each experiment was repeated 3 times independently with similar results. **b**, PaoP5Δ*dap1* mutant forms smaller plaques than WT PaoP5. Shown are 10-fold serial dilution plaque assays comparing the plating efficiency of WT and mutant phages on PAO1 and PAO1 containing *p-dap1* vector. **c**, Both PaoP5Δ*dap1* and PaoP5 phages

adsorbed to PAO1 efficiently. Data are mean ± s.d. of 4 biological replicates. NS, not significant, based on Student's *t*-test. **d**, One-step growth curve showing that PaoP5Δ*dap1* produces fewer progenies than PaoP5. **e**, The burst size of PaoP5Δ*dap1* and PaoP5 are 14.52 ± 3.62 p.f.u.s per cell and 104.95 ± 17.14 p.f.u.s per cell, respectively. Data represent mean ± s.d. (*n* = 3). Statistical significance was determined using a two-sided Student's *t*-test.

plating (EOP) of PaoP5Δ*dap1* in PAO1/*p-dap1* is similar to that in PAO1/EV (Fig. 2b). This indicates that *dap1* is important for phage fitness.

The phage life cycle starts from initial adsorption, whereas PaoP5Δ*dap1* and WT phage both bound to the host efficiently (*P* > 0.05), thus host binding is not the reason for the difference between phages (Fig. 2c). Next, we evaluated the burst size of the two phages because plaque size is associated with burst size[33]. The one-step growth curve experiment showed that PaoP5Δ*dap1* generated fewer progenies than PaoP5 (Fig. 2d). The burst sizes of PaoP5 and PaoP5Δ*dap1* were ~104.95 ± 17.14 plaque-forming units (p.f.u.s) per cell and 14.52 ± 3.62 p.f.u.s per cell (Fig. 2e), respectively. Thus, the number of progenies produced by PaoP5Δ*dap1* is only ~13.83% of that produced by the wild-type phage PaoP5.

Since Dap1 inhibits DipA, we thus infer that DipA might constrain the replication of PaoP5Δ*dap1*. However, the small plaque formation phenotype of PaoP5Δ*dap1* could not be rescued when it infected Δ*dipA* (Extended Data Fig. 6b), suggesting that the phage fitness conferred by Dap1 is independent of DipA even though Dap1 inhibits DipA.

DNA packaging in PaoP5Δ*dap1* is reduced
Since *dap1* is an early-expressed gene that promotes phage productivity, this led us to hypothesize that an unidentified antiphage defence system in PAO1 might inhibit phage productivity, and Dap1 could overcome this antiphage system. Thus, we used proteomic approaches to characterize

the impact of Dap1 on both phage proteins (Fig. 3a) and host proteins (Extended Data Fig. 7 and Supplementary Table 2). Two phage proteins (Orf049, Orf050) were downregulated in PaoP5Δ*dap1*-infected PAO1. The abundance of Orf050 in PaoP5Δ*dap1*-infected PAO1 was reduced to about one-tenth of the protein level in PaoP5-infected PAO1 (Fig. 3a). Orf50 is annotated as an HNH endonuclease, which is a vital component of phage DNA packaging machines and is required for the specific endonuclease activity of large terminase proteins[34].

Interestingly, PaoP5Δ*dap1* was able to form large plaques when *orf50*, but not *orf049*, was overexpressed (Fig. 3b), suggesting the effect of a decreased level of HNH on the reduced packaging of PaoP5Δ*dap1*. Consistent with a previous report[34], electron micrographs of negatively stained phage lysates revealed numerous empty phage particles resulting from the absence of DNA packaging for phage PaoP5Δ*dap1* lysate, and the expression of either *dap1* or *hnh* in PAO1 completely restored the DNA packaging efficiency to that of wild-type phage (Fig. 3c,d and Extended Data Fig. 8). These data indicate that when PaoP5Δ*dap1* infects PAO1, phage HNH endonuclease is significantly degraded, fewer capsids are packaged with phage DNA and fewer progenies are generated.

Lon protease defends PAO1 against PaoP5Δ*dap1*
These data indicate that Dap1 might protect HNH endonuclease from quick degradation. We hypothesized that the protease Lon of *P. aeruginosa* might be involved in degrading HNH endonuclease since
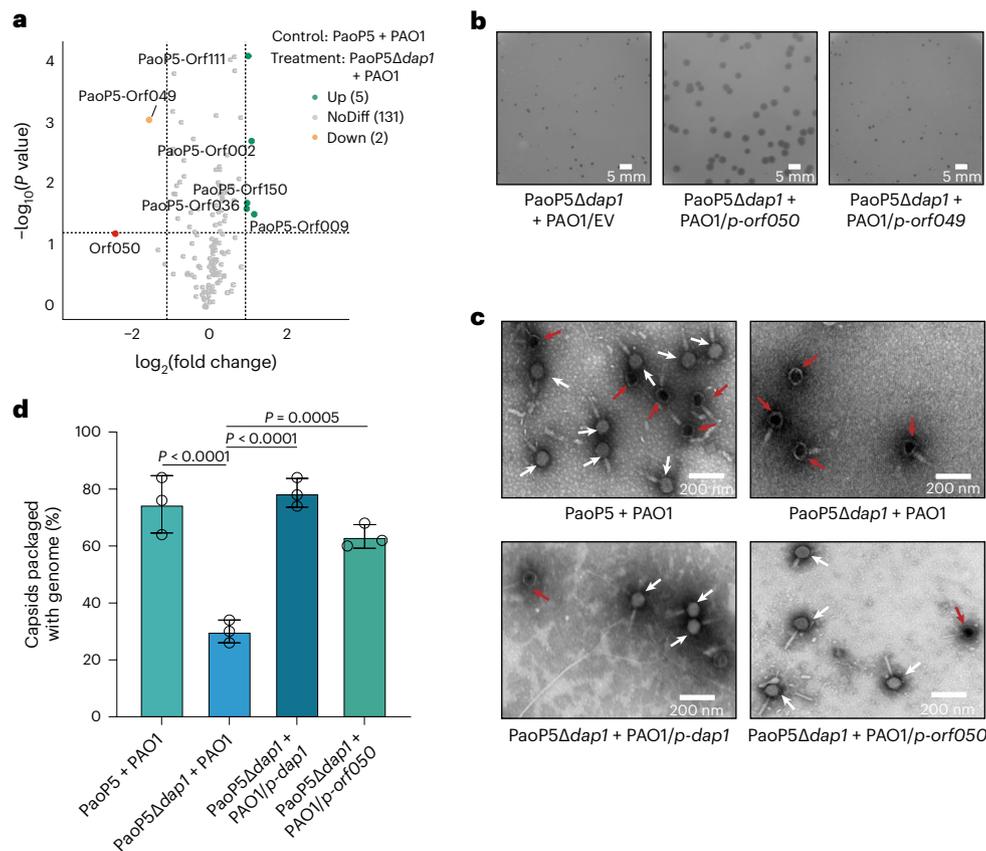
Fig. 3 | PaoP5Δ*dap1* is less efficient in genome packaging due to the decreased abundance of HNH endonuclease. a, The differentially expressed phage proteins between the PaoP5- and PaoP5Δ*dap1*-infected PAO1. Orf049 and Orf050 (HNH endonuclease) were significantly depressed in PaoP5Δ*dap1*-infected PAO1. Green dots, upregulated; orange and red dots, downregulated. *P* values were assessed using two-sided Fisher's exact test and adjusted for multiple hypothesis testing using the Benjamini–Hochberg correction; proteins with *P* < 0.05 were considered statistically significant. **b**, PaoP5Δ*dap1* infected with PAO1/*p-orf050* forms larger plaques than those infected with PAO1/EV or PAO1/*p-orf049*. Each experiment was repeated 3 times independently with similar results. **c**, Representative TEM of negatively stained phages produced in PAO1, PAO1/*p-dap1* or PAO1/*p-orf050*. Red arrows, the empty capsids; white arrows, the phages in which the genome is packaged. **d**, Phages were cultured in the indicated strains, and the percentage of capsids packaged with genomes was calculated from 3 biological repeats. Only 30% ± 3.27% of the PaoP5Δ*dap1* cultured in PAO1 are packaged with genomes, while complementation of *dap1* or *hnh* increased the rate to 78.67% ± 4.11% or 63.33% ± 3.44%, respectively. A total of 150 particles were counted for the presence or absence of the genome. Data represent mean ± s.d. (*n* = 3) and statistical significance was determined using one-way ANOVA with Dunnett's multiple comparisons test.

Lon was reported to cleave the proteins of prophages in *E. coli*[35]. To verify this hypothesis, PaoP5Δ*dap1* was used to infect wild-type PAO1 or Δ*lon* and our data showed that PaoP5Δ*dap1* formed larger plaques in Δ*lon* than in PAO1 (Fig. 4a). Moreover, the electron micrographs demonstrated that most progenies of PaoP5Δ*dap1* are packaged with DNA in Δ*lon* (Fig. 4b,c). Then, PaoP5Δ*dap1*-infected PAO1 or Δ*lon* were analysed by 4D label-free high-throughput proteomic assay, which showed a significant effect of Lon on host proteins, and 697 host proteins were identified as differentially expressed proteins (DEPs) (Supplementary Table 3). Among the phage proteins, the HNH endonuclease (Orf050) abundance was significantly increased in the PaoP5Δ*dap1*-infected Δ*lon* than that in PaoP5Δ*dap1*-infected PAO1 (Fig. 4d and Supplementary Table 3), indicating that without Lon, phage HNH endonuclease is not significantly degraded.

Our data suggest the functional role of *P. aeruginosa* Lon protease as a host-encoded phage-restriction protein. To test whether Lon is a common phage defence factor, we challenged PAO1 and Δ*lon* against three other *P. aeruginosa* phages (Supplementary Table 1). We found that Lon could inhibit *P. aeruginosa* phage PaP_Se (GenBank: OL441337.1) (Supplementary Table 1), as the phage titre increased by ~100-fold in the absence of Lon (Fig. 4e). However, overexpression of *dap1* could not increase the productivity of phage PaP_Se in PAO1, indicating that Lon might defend PAO1 against PaP_Se through other mechanisms that could not be overcome by phage Dap1. Overall, these data reveal the role of Lon protease in serving as a phage defence protein and inhibiting PaoP5Δ*dap1* and environmentally isolated phage PaP_Se.

Dap1 binds to HNH to prevent Lon-mediated HNH degradation

Since Lon protease reduced the abundance of HNH endonuclease, we performed an in vitro assay[36,37] and found that HNH endonuclease was degraded in the presence of both Lon protease and kinase (Fig. 5a).

Next, we attempted to determine whether Dap1 might directly bind to Lon to inhibit the protease activity[38,39]. Neither bacterial two-hybrid (Fig. 5b) nor Co-IP assays (Fig. 5c) revealed a direct interaction between Dap1 and Lon. This is not unexpected. As Lon is a vital protease[39], if Dap1 directly binds to Lon and interferes with its function, we would expect a growth defect in PAO1 overexpressing *dap1*, which is not the case (Extended Data Fig. 1b). Thus, our data indicate that Dap1 does not bind to Lon to inhibit its protease activity. We then proposed that Dap1 might bind to HNH endonuclease to prevent Lon-mediated HNH degradation. As expected, both the BACTH (Fig. 5b) and pull-down assays (Fig. 5d) detected the binding of Dap1 to HNH, and the in vitro protein degradation assays showed that Lon degraded Dap1; however, when Dap1 was premixed with HNH, the degradation of the Dap1–HNH mixture was reduced (Fig. 5e). Collectively, the biochemical and
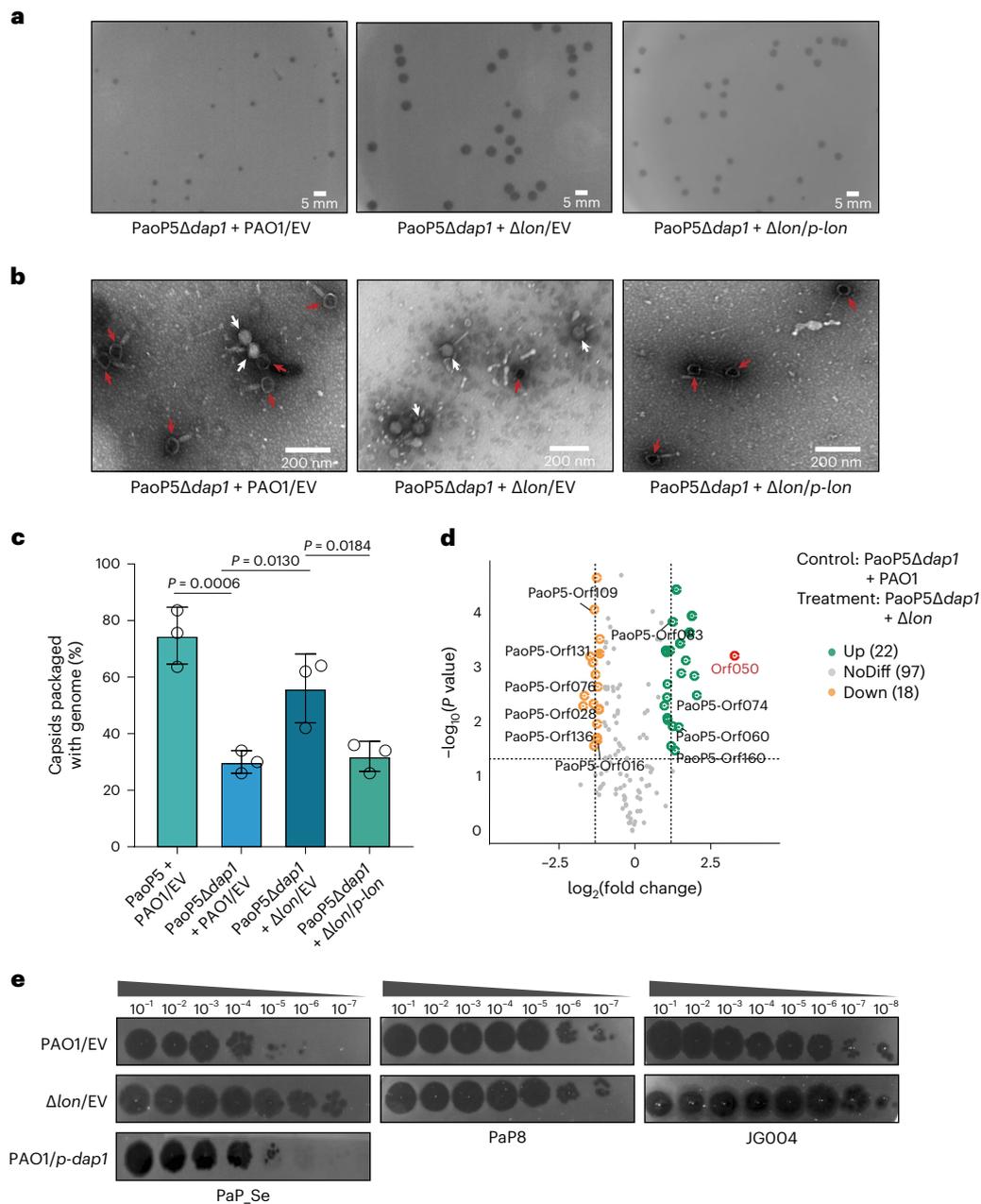
Fig. 4 | Lon protease decreases the abundance of HNH endonuclease and inhibits phage genome packaging of PaoP5Δ*dap1*. a, PaoP5Δ*dap1* forms large plaques on Δ*lon* but forms tiny plaques in Δ*lon*/*p-lon*. **b**, Representative transmission electron micrographs of negatively stained phages produced in PAO1 and Δ*lon*. Red arrows, the empty capsids; white arrows, the phages in which the genome is packaged. **c**, Phages were cultured in the indicated strains, and the percentage of capsids packaged with genomes was calculated from 3 biological repeats. A total of 150 particles were counted for the presence or absence of the genome. Data represent mean ± s.d. (*n* = 3) and statistical significance was determined using one-way ANOVA with Dunnett's multiple comparisons test. **d**, Volcano plot of the DEPs for PaoP5Δ*dap1* infected with either PAO1 or Δ*lon* analysed by LC–MS/MS. Green and red dots, upregulated; orange dots, downregulated. **e**, The EOP of phage PaP_Se increased ~100-fold when *lon* was deleted, but overexpression of *dap1* did not increase the EOP of PaP_Se. In contrast, the EOP of phage PaP8 and JG004 on PAO1 and Δ*lon* were similar. Each experiment was repeated 3 times independently with similar results.

genetic studies indicate that Dap1 binds to HNH to protect it from Lon-mediated degradation.

Dap1 is essential for the efficacy of phage therapy

To further characterize the impact of *dap1* on phage fitness, we performed a competition assay and found the relative abundance of PaoP5 and PaoP5Δ*dap1* to be 94.67% ± 2.62% and 3.33% ± 2.62%, respectively (Fig. 6a). Moreover, PaoP5Δ*dap1* was outcompeted by two other environmentally isolated phages (PaP8 and JG004) (Fig. 6a). Together, this result suggests that PaoP5Δ*dap1* is at a significant disadvantage when competing with other phages that infect the same host, indicating that *dap1* is critical for the survival of PaoP5-like phages in the natural environment.

We further tested the impact of Dap1 on phage therapy using the mouse model. A single dose of phage PaoP5 at a multiplicity of infection (MOI) of 10 rescued 100% of *P. aeruginosa* intraperitoneally infected mice (Fig. 6b). However, when the *P. aeruginosa* intraperitoneally infected mice were treated with a single dose of phage PaoP5Δ*dap1*, all the mice died within 7 days, although the mice exhibited delayed time-to-death (Fig. 6b).
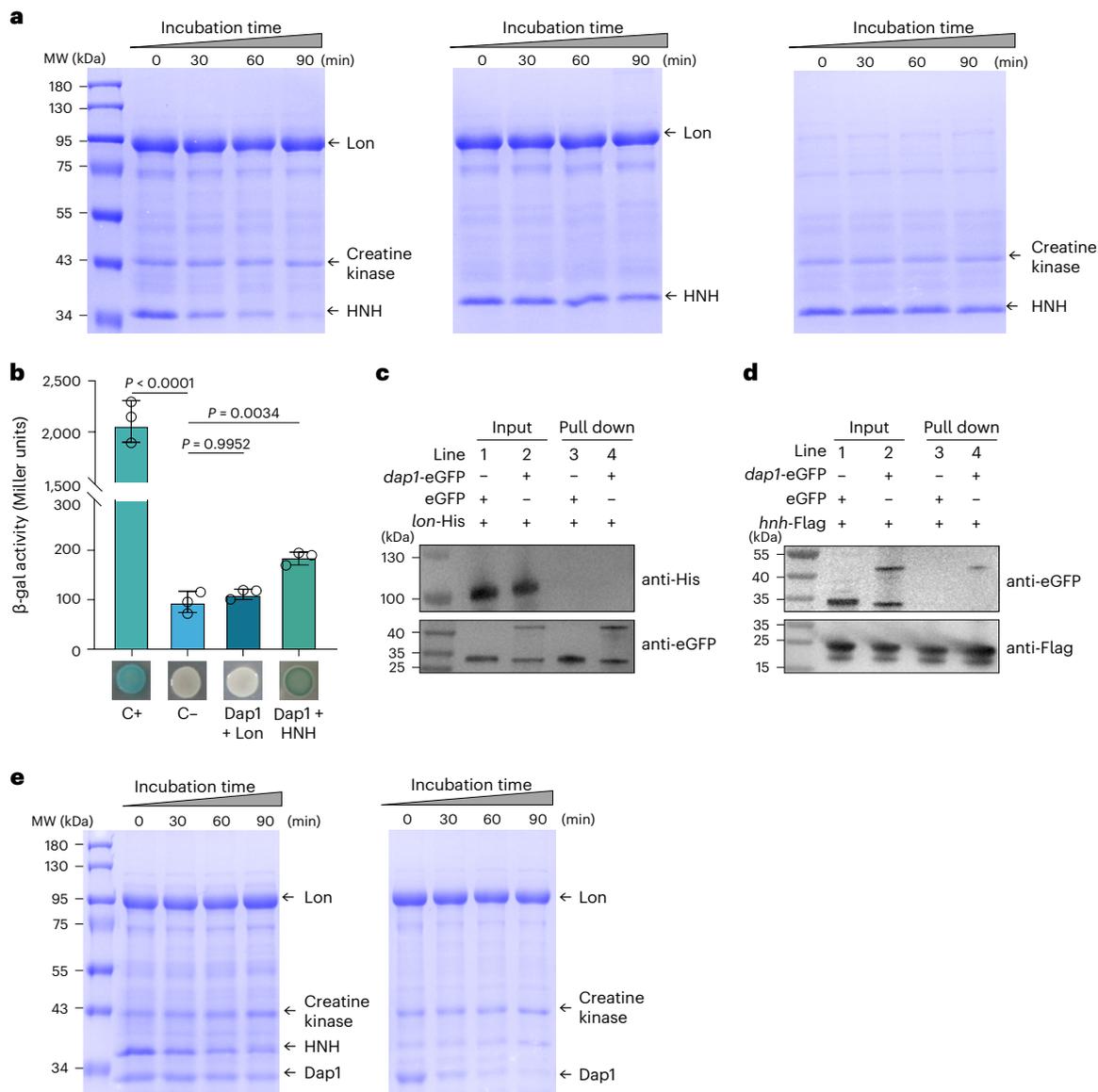
Fig. 5 | Dap1 binds to HNH endonuclease to prevent Lon-mediated HNH degradation. a, Representative images of SDS–PAGE gels of in vitro degradation of HNH by Lon protease in the presence of ATP and creatine kinase. **b**, Bacterial two-hybrid assay indicates that Dap1 interacts with the HNH endonuclease but not with Lon. Interactions were visualized by a drop test on LB agar plates, and the presence of a blue colony was an indication of positive interaction and quantified by measuring the β-galactosidase activity. Data represent mean ± s.d. ($n = 3$) and statistical significance was determined using one-way ANOVA with Dunnett's multiple comparisons test. **c**, Co-IP assays show no interaction between Dap1 and Lon. Overnight cultures of *E. coli* containing *lon*-His with either eGFP or *dap1*-eGFP were lysed. Cell-lysis supernatants were incubated with anti-eGFP beads and then proteins were detected by western blot with His or eGFP antibody. **d**, Co-IP assays show that Dap1 binds to HNH. Overnight cultures of *E. coli* containing HNH-Flag with either eGFP or *dap1*-eGFP were lysed. Cell-lysis supernatants were incubated with anti-Flag beads and then proteins were detected by western blot with Flag or eGFP antibody. **e**, In vitro proteolysis assay shows that Lon degrades Dap1, but the HNH/Dap1 mixture is degraded much slower by Lon. Protein samples taken at indicated time points were subsequently visualized by 12% SDS–PAGE and Coomassie staining. All experiments were repeated at least 3 times with similar results and representative figures are shown.

To further evaluate the efficacy of PaoP5Δ*dap1* and PaoP5, we examined the phage titre and bacterial c.f.u.s in the liver after phage therapy[40]. As shown in Extended Data Fig. 9a, significantly more phages were detected in the liver in the PaoP5-treated, PAO1-infected mice. The titre peaks at 8 h (-1.75×10^8 p.f.u.s g^{-1}) and the bacterial c.f.u.s in the liver were cleared within 96 h. In contrast, PaoP5Δ*dap1* titres decreased rapidly, reaching undetectable levels by 72 h and the bacterial c.f.u.s in the liver continued to increase post infection (Extended Data Fig. 9b).

To assess whether phage resistance was the cause of failed treatment with PaoP5Δ*dap1*, 200 colonies isolated from the dead mice were evaluated for phage resistance (Extended Data Fig. 9c). Overall, 41% of these strains were phage-sensitive *P. aeruginosa*, 39%

were phage-resistant *P. aeruginosa*, while the other phage-resistant strains are gut commensal bacteria, such as *Enterobacter hormaechei* and *Escherichia coli*, which might translocate to the liver after systemic bacterial co-infections (Extended Data Fig. 9c)[41,42]. Therefore, phage-resistant mutants were observed in the PaoP5Δ*dap1*-treated mice, which might also have contributed to the death of the mice. These data indicate that *dap1* is essential for the efficacy of phage therapy, and self-replication to produce enough progenies to infect and clear bacteria quickly is critical for successful phage therapy.

Next, we searched the homologous genes in the National Center for Biotechnology Information (NCBI) to investigate the prevalence of *dap1* and *hnh* genes among *P. aeruginosa* phages. Among the
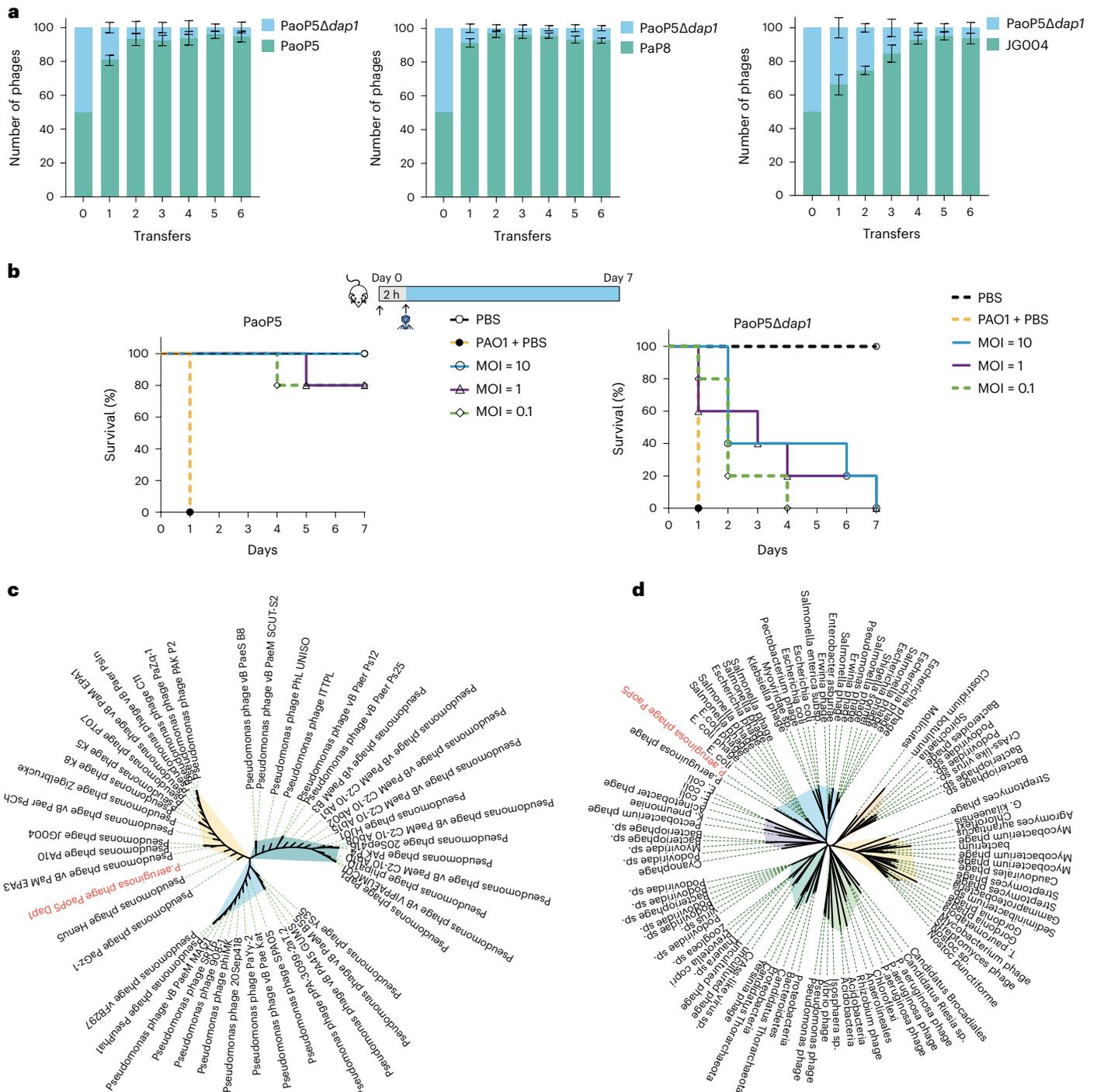
Fig. 6 | Dap1 is essential for the fitness of phage and the efficacy of phage therapy. a, Competition assay between PaoP5Δ*dap1* and the WT phages. Three biological repeats were performed. **b**, Survival of 7-week-old BALB/c mice (*n* = 5) following intraperitoneal injection with PAO1 and phage PaoP5Δ*dap1* or PaoP5 at an MOI of 10, 1 and 0.1. **c**, Phylogenetic tree of Dap1 homologues with minimal identity of 90%. The phylogenetic tree was generated using neighbour-joining analysis by MEGA 7. Evolutionary distances were computed using the *p*-distance method, and the black line represents the number of substitutions per site. **d**, Phylogenetic tree of the HNH homologues in the phage genomes generated using neighbour-joining analysis by MEGA 7. Evolutionary distances were computed using the *p*-distance method. The black line represents the number of substitutions per site, and the green dashed line indicates each strain or bacteriophage. Different coloured shadings represent different clades, which are mainly for aesthetic purposes.

785 sequenced *Pseudomonas* phages as of October 2023, 50 carried homologous genes of *dap1*, and the 48 *dap1*-like phage genes with a minimal identity of 90% were clustered into three clades according to the phylogenetic relationships (Fig. 6c). Specifically, *dap1* is relatively conserved among the PAK_P1-like phages, and over 40% (25 out of 62) of PAK_P1-like phages encode homologous genes of *dap1*. As to the *hnh* genes, 99 HNH endonucleases with a minimal identity of 30% to ORF050 were predicted by BLAST and were clustered into 7 clades (Fig. 6d). These bioinformatics analyses indicated that *dap1*-like genes are conserved among a subgroup of *P. aeruginosa* phages.

Discussion

Phages are absolute parasites that rely heavily on bacteria for reproduction. Thus, phages have numerous strategies to modulate host metabolism[17,18]. However, phage proteins affecting bacterial virulence are not well investigated and these targets might lead to the development of antivirulence therapies[43–46]. In this study, we systematically investigated the impact of PaoP5 lytic phage proteins on bacterial host PAO1. In addition to the 7 lethal phage proteins whose overexpression led to drastic bacterial growth inhibition, we identified Dap1 which enhanced the intracellular c-di-GMP level by binding to bacterial c-di-GMP phosphodiesterase DipA and interfering with its function, leading to the inhibition of bacterial swimming/swarming motility and enhancing biofilm formation (Fig. 1b,c). Notably, the inhibition of DipA by phage Dap1 significantly attenuated bacterial virulence in a mouse model of acute infection (Fig. 1h), indicating that phage may modulate host pathogenesis via its encoded function. Therefore, these findings might serve as a model for developing small-molecule or peptide-based antivirulence compounds for *P. aeruginosa*.

While the function of Dap1 in helping lytic phage evade the Lon protease-mediated antiphage immunity by binding to HNH is of biological relevance (Fig. 6a), the biological significance of the interaction between Dap1 and DipA is less clear. Since the phage is non-motile, the reduced movement of the infected bacteria might reduce the chance of encountering other phages and therefore ensure that the preyed bacteria are not shared by other phages[47], conferring an advantage for PaoP5. Thus, the increased c-di-GMP level resulting from Dap1 function might increase phage fitness via yet-to-be-determined mechanisms. Overall, the significance of DipA and Dap1 interaction on phage is not clear yet, and further study is warranted[48].

Our study also identified Lon protease as an element in antiphage defence. The role of proteases in antiphage defence is poorly studied[10,49]. Several proteases in phage defence systems function by activating effectors that induce the death of the phage-infected bacteria[15,16]. Our data demonstrated that Lon protease could efficiently cleave phage HNH endonuclease to inhibit genome packaging of PaoP5Δ*dap1*, thus serving as an antiphage element. We further demonstrated that phage-encoded Dap1 may serve as a countermeasure to evade Lon protease-mediated antiphage defence (Extended Data Fig. 10). Several lytic phage proteins have been reported to bind to proteases and inhibit the proteolysis function of proteases[38,39]. However, the benefits of phages inhibiting host protease are not well investigated. We showed that rather than directly binding to Lon protein to inhibit its proteolytic function (Fig. 5c), Dap1 binds to phage HNH to alleviate the Lon-mediated protein degradation (Fig. 5e).

By protecting HNH endonuclease from Lon-mediated degradation, Dap1 ensures effective DNA packaging and generation of a high number of phage particles during PaoP5 infection of PAO1. The ability to produce large numbers of progeny by lytic phage may not only offer a competitive advantage in natural environments as demonstrated by our competition assay but is also critical in achieving high efficacy when being used for phage therapy (Fig. 6b). Furthermore, the well-conserved *dap1* gene among 50 PaoP5-like phages isolated from different countries supports our hypothesis that this gene may indeed be important in conferring fitness advantage in the natural environment.

Phages are promising alternatives to treat clinical bacterial infections[50,51]. For phage therapy, we tend to use phage cocktails or combine phage with antibiotics to improve the efficacy of phage therapy[52,53]. Moreover, we tend to choose phages that induce large plaque formation and have high lysis efficiency. However, the genetic determinants that lead to these characteristics have not been well studied. Here we demonstrate that *dap1* is a genetic factor that is important for conferring high phage lysis efficiency, and PaoP5 forms large plaques on some clinical strains while PaoP5Δ*dap1* forms small plaques (Extended Data Fig. 9d).

Moreover, Dap1 could also enhance the success rate of phage therapy. We found that (1) PaoP5Δ*dap1* is less efficient in treating infections (Fig. 6b), (2) PaoP5Δ*dap1*-treated mice had lower liver phage titre than PaoP5-treated mice and (3) the bacteria were not effectively cleared in PaoP5Δ*dap1*-treated mice. We also detected the appearance of phage-resistant *P. aeruginosa* mutants that might also have contributed to the death of the mice (Extended Data Fig. 9c). Thus, the phage resistance mechanism and its impact on antibiotic resistance patterns deserve further investigation. These data indicate that efficient replication of phage to release enough progenies is essential for the success of phage therapy and prove that efficient self-replication is an advantage and critical factor for the success of phage therapy.

In conclusion, this study reveals the remarkable dual-functional feature of phage protein Dap1 that could target both host protein DipA and phage protein HNH−two unrelated proteins that function in bacteria and phage, respectively. Our finding also highlights the immense evolution pressure on phages to control host function and overrun the host-encoded phage defence systems to persist and co-exist with their bacterial hosts within natural niches.

Methods

Bacterial strains, phages and culture conditions

The bacterial strains, phages and plasmids utilized in this study are documented in Supplementary Table 1. The strains of *E. coli* and *P. aeruginosa* were cultivated on Lysogeny Broth (LB) medium at 37 °C with 220 r.p.m. shaking. The following concentrations of antibiotics were used when necessary: for *E. coli*, carbenicillin at 100 µg ml⁻¹, kanamycin at 50 µg ml⁻¹, tetracycline at 10 µg ml⁻¹; for *P. aeruginosa* PAO1, carbenicillin at 300 µg ml⁻¹, tetracycline at 100 µg ml⁻¹ and gentamicin at 50 µg ml⁻¹. Bacteriophages were cultivated with host bacteria in LB medium at 37 °C.

Plaque and EOP assay

The phage plaque assay was conducted according to a previously published protocol[54]. In brief, 200 µl of bacterial culture in the log phase (optical density at 600 nm (OD_{600}) of 0.6) was combined with 100 µl of diluted phages (~100 p.f.u.s) and 4 ml of 0.4% LB agar. This mixture was subsequently overlaid onto LB agar plates and cultured overnight at 37 °C until the formation of plaques occurred. The EOP of phages on various bacteria was determined as previously described[55] (Supplementary Table 1). LB agar (4 ml, 0.4%) was combined with 200 µl of log-phase bacterial culture (OD_{600} of 0.6) and poured onto the LB agar plates. Volumes of 2 µl of serial 10-fold dilutions of a phage solution were spotted on the double-layer agar plates and then incubated for 18 h at 37 °C until plaques formed. The host range of PaoP5 among 233 clinical *P. aeruginosa* strains was tested using plaque assay[56]. A volume of 200 µl of bacterial culture in the log phase (OD_{600} of 0.6) was combined with 4 ml of 0.4% LB agar and overlaid onto LB agar plates. Then, 5 µl of phage PaoP5 was spotted on the plates and cultured overnight at 37 °C. The formation of clear plaques indicates that the strain is sensitive to PaoP5.

Overexpression of genes in *P. aeruginosa*

To express the phage gene *orf003* in the PAO1 strain, a DNA fragment was generated by PCR using the *orf003*-F and *orf003*-R primer pair, as outlined in Supplementary Table 2. The PCR products were digested using the restriction enzymes *Eco*RI and *Hin*dIII. Subsequently, the resulting digested fragment was ligated with the *Eco*RI/*Hin*dIII-digested pME6032 vector, yielding *p-dap1*. The resultant plasmid *p-dap1* was then introduced into the PAO1 strain. The colonies that grew on the plate containing tetracycline were transferred into culture conditions supplemented with 1.0 mM IPTG to induce the expression of the cloned genes. The other 59 genes of PaoP5 were cloned using the identical methodology with the corresponding primers listed in Supplementary Table 2.

The arabinose-inducible *pHERD20T-orf050* plasmid was constructed using the Gibson assembly method. The *orf050* gene was amplified by PCR using the *pHERD-orf050*-F and *pHERD-050*-R primer pair. The PCR product was ligated with the pHERD20T vector. Subsequently, the resultant plasmid was introduced into the PAO1 strain by electroporation. The colonies were formed on a plate supplemented with gentamicin. A 0.2% concentration of arabinose was used to induce the expression of *orf050*. PAO1/*p-orf049* was constructed using the same approach, employing the primers described in Supplementary Table 2. The plasmid *pUCP24-dap1* was constructed as described above.

Knockout of dipA in *P. aeruginosa*

A SacB-based approach was used to knockout *dipA* in PAO1, as previously mentioned[57]. The upstream (1,061 base pairs) and downstream (1,051 base pairs) fragments of the intended deletion was amplified by PCR using the primer pairs *dipA*-up-F/*dipA*-up-R (*Bam*HI/*Xba*I) and *dipA*-down-F/*dipA*-down-R (*Xba*I/*Hin*dIII), respectively (Supplementary Table 2). The two PCR products were digested using the restriction enzymes *Bam*HI/*Xba*I and *Xba*I/*Hin*dIII and then cloned into the same enzyme-digested gene replacement vector pEX18Amp, yielding *pEX18Ap-dipA*. The resultant plasmids were electroporated into PAO1 with selection for carbenicillin resistance. Subsequently, colonies exhibiting carbenicillin susceptibility and sucrose resistance were collected on LB agar plates containing 300 µg ml^{-1} carbenicillin and 10% sucrose. This dual phenotype implies a double-crossover event and consequently indicates gene replacement occurrence. The *dipA* deletion was verified by PCR.

Bacterial growth curves

The bacterial cultures were grown overnight and diluted at a ratio of 1:100 in fresh medium. Subsequently, 100 µl of the cultures supplemented with tetracycline (100 µg ml^{-1}) and IPTG (1.0 mM) were carefully deposited into 96-well plates. The plates were then placed in an incubator set at 37 °C and subjected to gentle shaking at 100 r.p.m. The OD_{600} was determined for each well using a microplate spectrophotometer (Thermo Scientific) at regular intervals of 2 h for a total duration of 24 h. A total of 3 biological replicates were conducted.

Development of biofilm in flow chamber

The biofilm fluorescence microscopy experiment was performed as previously reported[58]. Briefly, bacterial strains were cultivated in LB medium for 36 h at 37 °C in flow chambers. Subsequently, SYTO9 (Thermo Fisher) was used to stain the total biofilm, which was then subjected to confocal microscopy imaging (LSM780, Carl Zeiss).

Static biofilm assay

The biofilms were analysed using crystal violet staining as previously described[59]. Briefly, log-phase bacterial cultures were diluted 1:100 in LB medium. Aliquots (2.0 ml) were incubated in 10 ml borosilicate tubes for 18 h at 25 °C. Biofilms were stained with 0.1% crystal violet for 30 min and tubes were washed with water to remove unbound dye. The remaining crystal violet was dissolved in 2.0 ml of 95% ethanol and this solution was measured at a wavelength of 595 nm (OD_{595}) using a SpectraMax M3 multimode microplate reader.

Swimming and swarming motility assays

The motility assays were carried out as previously described[57]. The swimming medium consisted of 0.8% nutritional broth, 0.5% glucose and 0.5% agar, while the swarming medium was composed of 1% tryptone, 0.5% NaCl and 0.3% agar. Subsequently, 2.0 µl of overnight bacterial cultures was spotted onto agar plates and incubated at 37 °C for 16 h.

RNA-seq and data analysis

The PAO1/EV and PAO1/*p-dap1* strains were cultured in LB medium at 37 °C until OD_{600} reached ~0.6. Total RNA was immediately extracted using TRIzol reagent according to manufacturer instructions (Invitrogen). The Ribo-Zero rRNA removal kit was employed to eliminate ribosomal RNA. Following this step, complementary DNA libraries were constructed, and the resulting libraries were subjected to sequencing using an Illumina HiSeq 2500 sequencer. Each sample in the RNA-seq assay was sequenced three times. RNA-seq reads were mapped to the *P. aeruginosa* genomes (NC_002516.2) provided by NCBI using Bowtie2 and only the uniquely mapped reads were kept for subsequent analyses. DEGs were identified using DESeq2 (Benjamini–Hochberg-adjusted $P < 0.05$ and $|\log_2(\text{fold change})| > 1$)[60]. The data have been uploaded to BioProject under accession number PRJNA1020646.

RT–qPCR

To validate the RNA-seq data, PAO1 and PAO1/*p-dap1* samples were prepared as described above. To validate the expression of *dap1*, 10 ml of bacterial PAO1 culture ($OD_{600} = 0.6$) was infected with phage at an MOI of 10 and the culture was grown at 37 °C with shaking. For RNA extraction, 1 ml of the culture was taken at given time points (1 and 10 min). Three biological repeats were performed.

RNA extraction was performed as previously described[61]. Briefly, total RNA was extracted from each sample using an RNAprep Pure Cell/Bacteria kit (TIANGEN), rRNA was removed and cDNA was generated using the PrimerScriptTM RT reagent kit with gDNA eraser (Takara). RT–qPCR was performed using 2X Universal SYBR Green Fast qPCR Mix (ABclone). The primers used in this study are listed in Supplementary Table 1. The 16S rRNA gene was used as the reference gene for normalization and the expression of each gene was compared using the delta-delta Ct method.

Bacterial two-hybrid assay

The bacterial two-hybrid analysis was carried out as previously described[28]. Forty-two genes were individually cloned into the BACTH plasmid pKT25 and *dap1* was cloned into pUT18C with primer pairs (Supplementary Table 2). The *pUT18C-zip* and *pKT25-zip* strains were used as the positive control, while the non-fused T25 and T18 domains were used as the negative control. Subsequently, the corresponding pUT18C and pKT25 constructs were transformed into *E. coli* BTH101 cells and then spread onto LB plates that were supplemented with 50 µg ml^{-1} kanamycin, 100 µg ml^{-1} ampicillin, 1 mM IPTG and 40 µg ml^{-1} 5-bromo-4-chloro-3-indolyl-β-D-galactopyranoside (X-gal). The plates were subjected to incubation at 30 °C for 2 days and blue colonies indicated positive interaction. The quantification of β-galactosidase activity was performed using Miller assays as previously described[26].

Co-IP assay

E. coli cells containing *dipA*-Flag with either eGFP-tagged *dap1* or eGFP were grown in LB medium supplemented with 0.5 mM IPTG. After reaching the stationary phase, 30 ml of the bacterial cultures were collected and resuspended in IP lysis buffer (10 mM Tris-HCl (pH 7.5), 2 mM EDTA, 1% NP-40 and 150 mM NaCl). In addition, protease and phosphatase inhibitors were added to the lysis buffer. Subsequently, each sample underwent lysis using sonication for 10 min at 4 °C. All supernatants were then gathered and subjected to filtration using a 0.22 µm filter. The lysates were subjected to incubation with Flag beads on a rotator for 4 h at 4 °C and the beads were washed five times using IP buffer, followed by denaturation in 1X SDS loading buffer. Proteins were separated using SDS–PAGE and subsequently subjected to immunoblotting using monoclonal antibodies against eGFP and Flag. The Co-IP experiments involving the interaction between Dap1 with RocR, ProE, Lon and HNH endonucleases were conducted following the same methodology. Antibody-related information is listed in Supplementary Data 4.

Quantification of c-di-GMP by LC–MS

Extraction of c-di-GMP from *P. aeruginosa* cells was performed as previously described[62,63] with minor modification. Briefly, 10 ml of

bacterial suspension was centrifuged at 8,000 g and 4 °C for 2 min. The pellet was transferred and resuspended in 5 ml of phosphate-buffered saline (PBS). After centrifugation, the pellet was washed twice and resuspended in 5 ml of extraction buffer (methanol:acetonitrile:water at 2:2:1). The suspension was flash frozen in liquid nitrogen and thawed before vortexing until no visible bacteria remained. The suspension was then sonicated for 5 min at low temperature. The resulting liquid was centrifuged at 12,000 g and 4 °C for 30 min and the supernatant was freeze dried to a powder using a CentriVap benchtop vacuum concentrator at 4 °C. The powder was resuspended in 200 μl of extraction buffer and centrifuged at 12,000 g and 4 °C for 10 min. The supernatant was transferred to a mass spectrometry sample tube for analysis. Identification and relative quantification of c-di-GMP were performed using a triple quadrupole mass spectrometer (Q-Exactive, Thermo Fisher). Standards were dissolved in water and separated on a C18 column using a binary pump system with solvent A consisting of water containing 0.1% (v/v) formic acid and eluent B consisting of acetonitrile containing 0.1% (v/v) formic acid. The gradient started at 10% eluent B and was held for 10 min at a flow rate of 0.3 ml min^{-1}. The column temperature was maintained at 30 °C and the autosampler temperature was set at 4 °C. Data were analysed using Xcalibur (v.4.0) and Trace Finder (v.4.1). The c-di-GMP levels were normalized to total protein per ml of culture. Data represent averages of three independent cultures.

Mouse infection and phage therapy experiment

The Animal Research Ethics Committee of the Army Medical University reviewed, approved and supervised the protocols for animal research (permit number: AMUWEC20230178, AMUWEC20230470). The mice were purchased from Hunan SJA Laboratory Animal Company and housed under specific pathogen-free conditions; the housing environment had controlled temperature (20–26 °C), humidity (40–70%) and lighting conditions (12 h light and 12 h dark cycle), and no animal was excluded from the analyses. For the mouse infection experiment, PAO1/*pUCP24* and PAO1/*pUCP-dap1* strains were grown in LB medium at 37 °C until the early stationary phase. Cells were collected and resuspended in PBS to OD$_{600}$ of 0.6. Of each strain, 100 μl (~2 × 10^7 c.f.u.s), or 100 μl of PBS (negative control), was intraperitoneally inoculated into 7-week-old BALB/c female mice, and mice were monitored every 24 h for 120 h (5 days), with each group comprising 10 mice. At 5 days after infection, mice that survived the initial challenge were euthanized.

For the phage therapy experiment, 7-week-old BALB/c female mice were intraperitoneally inoculated with 50 μl of bacteria (~6 × 10^7 c.f.u.s) or 50 μl of PBS (negative control). After 2 h, 50 μl of phage PaoP5 or PaoP5Δ*dap1* (~6 × 10^8 p.f.u.s, ~6 × 10^7 p.f.u.s or ~6 × 10^6 p.f.u.s) was intraperitoneally inoculated into the infected mice. Each group included 5 mice, which were observed for 7 days. At 7 days after infection, mice that survived the initial challenge were euthanized.

To quantify the phage and bacteria in the liver, we determined the phage and bacterial counts for up to 96 h because phage will not be detectable after 4 days[39]. Thirty-two mice were treated with PaoP5, and 80 mice were treated with PaoP5Δ*d*ap1 because some of the mice died during the experiment and only the surviving mice were selected to quantify the bacteria and phage. Four mice from each group were euthanized by cervical dislocation at 1, 4, 8, 12, 24, 48, 72 and 96 h after phage administration. The liver tissue was homogenized as described previously[40]. To determine the phage titre, the homogenized liver tissue was centrifuged at 10,000 × g for 10 min and the phage titre in the supernatant was determined using the EOP assay as previously described[40]. For bacterial count, 100 μl of 10-fold serially diluted tissue sample was spread on LB agar plates in duplicates and incubated at 37 °C for 16 h.

The bacterial colonies isolated from the liver of the dead mice at 48 h after phage PaoP5Δ*dap1* therapy were tested for phage sensitivity using plaque assay. 16S rDNA sequencing was used to identify the species of the 30 phage-resistant colonies isolated from the liver of the dead mice.

Knockout of phage genes using the CRISPR-Cas9 system

The CRISPR-Cas9 plasmid pPTCS was applied to knock out phage genes as previously described[64]. To delete *dap1* in phage PaoP5, the spacer was generated by annealing primers *003*-G2-F/R (Supplementary Table 2) and ligated into the *Eco*31I-digested pPTCS plasmid. To construct the recombination template, primers Δ*003*-LA-F/R and Δ*003*-RA-F/R were used to amplify a 301 and 260 bp fragment before and after the *dap1* gene, respectively, and ligated into the multiple cloning site of pTCPLS by Gibson assembly. The resultant plasmid was then transferred into PAO1 to generate PAO1/pTCPLS-Δg003G2D, infected with 10^5 p.f.u.s of phages, and survivors selected using a plaque assay. The mutant phage was verified by PCR, followed by Sanger sequencing. Knockout of *orf014* or *orf153* in phage PaoP5 was performed with similar technology, with primers listed in Supplementary Table 2.

Bacteriophage adsorption assay

A phage adsorption assay was performed as previously described[65]. At an MOI of 0.01, the phage PaoP5Δ*dap1* or PaoP5 was mixed with *P. aeruginosa* PAO1 (OD$_{600}$ of 0.6). The mixture was centrifuged after being cultured for 10 min at 37 °C. Then, the phage titres in the original phage solution (t_1) and the supernatant (t_2) were ascertained using the double-agar plating tests. The formula for calculating the phage adsorption rate was (t_1–t_2)/t_1. Statistical significance was determined using Student's t-test on three biological replicates.

One-step growth curve of phages

The one-step growth curve of PaoP5 and PaoP5Δ*dap1* was determined as previously described[33]. Briefly, phage was combined with 1 ml of log-phase bacteria at an MOI of 0.01, and the mixture was incubated for 10 min at 37 °C. Following a 1 min 10,000 × g centrifugation of the combination, the pellet was resuspended in 100 ml of LB liquid medium and kept at 37 °C for 60 min. Every 10 min, 0.2 ml of the medium was moved to a fresh tube, which was then pelleted for 1 min at a speed of 10,000 × g. The phage titre in the supernatant was then immediately determined using the EOP assay. The burst size was defined as the ratio of the total number of phages released at the end of a growth cycle (40 min) to the total number of infected bacteria. For each phage, the tests were performed in triplicate.

Proteomics and data analysis

A total volume of 5 ml of PAO1 cultures with an OD$_{600}$ of 0.6 was combined with either PaoP5Δ*dap1* or PaoP5 at an MOI of 10 for 10 min. In addition, 5 ml of Δ*Lon* culture with an OD$_{600}$ of 0.6 was subjected to infection by PaoP5Δ*dap1* at an MOI of 10 for 10 min. Subsequently, 1 ml of the sample was subjected to centrifugation and the pellets were subjected to lysis using the SDT buffer (4% SDS, 100 mM Tris-HCl, 1 mM dithiothreitol, pH 7.6). Trypsin was used to break down the protein and C18 Cartridges (Empore TM SPE Cartridges C18 (standard density), Sigma) were then used to desalt the mixture. Following digestion, the peptides were concentrated by vacuum centrifugation and reconstituted in 40 μl of 0.1% v/v formic acid. The samples were analysed using LC–MS/MS. Protein sequences of the DEPs were searched using the NCBI BLAST+ client software and blasted against the online KEGG database (http://geneontology.org/) to map to pathways in KEGG.

TEM

The phage PaoP5Δ*dap1* or PaoP5 was cultured on various strains including PAO1, PAO1/*p-orf050*, PAO1/*p-dap1*, Δ*lon* or Δ*lon*/*p-lon*. The phage lysate was examined using TEM following established protocol[66]. The phage lysate was dropped onto carbon-coated copper grids for 10 min and subjected to negative staining using a 2% phosphotungstic acid solution for 30 s. Then, the phage particles were examined via TEM and the proportion of phages in which the capsids contained the genome was determined by calculating the average of over 50 particles from 3 separate biological replicates.

Protein expression and purification

To construct the *pET28a-dap1*, *pET28a-hnh* and *pET28a-lon* plasmids, the fragments of *dap1, hnh* and *lon* were amplified by PCR with the corresponding primers listed in Supplementary Table 2. Subsequently, the amplified fragment was digested with corresponding enzymes and ligated into pET28a vector. The resultant plasmids were introduced into *E. coli* BL21(DE3). After this, the strains were cultured in LB medium at 37 °C. When the OD_{600} reached 0.6–0.8, 0.5 mM IPTG was added to induce protein production. The cultures were incubated at 16 °C for an additional 20 h.

The cells were collected via centrifugation, resuspended in buffer A (20 mM tris-HCl (pH 8.0), 300 mM NaCl and 25 mM imidazole), lysed by high-pressure homogenization and centrifuged. The supernatant was applied to a 5 ml HisTrap HP column (Cytiva) and the target protein was eluted via AKTA purifier (GE Healthcare) using buffer B (20 mM tris-HCl (pH 8.0), 300 mM NaCl and 500 mM imidazole). The target protein was collected and applied to a HiLoad 16/600 Superdex 75 pg gel filtration column (Cytiva) equilibrated with buffer composed of 20 mM tris-HCl (pH 8.0), 200 mM NaCl and 2 mM dithiothreitol. The purified proteins were concentrated and stored at −80 °C.

Protein degradation assay

The HNH endonuclease degradation assay was performed as previously described[36,37]. Dap1 (100 µM) and HNH endonuclease (100 µM) were combined in a 1:1 ratio and left to react for 20 min on ice. Following this, the reactants were mixed with 30 µg of Lon in a 50 µl reaction buffer that contained 4 mM ATP, 50 mM Tris-HCl (pH 8.0), 10 mM $MgCl_2$, 1 mM dithiothreitol, 80 µg ml^{-1} creatine phosphokinase (Sigma, C3755) and 50 mM creatine phosphate (Sigma, 27920). The reaction mixture was incubated at 37 °C following the indicated time and a 10 µl aliquot was withdrawn. Subsequently, SDS–PAGE loading buffer was added to the mixture and the mixture heated for 15 min at 100 °C. The degradation of HNH was then observed using 12% SDS–PAGE. The analysis of HNH or Dap1 protein degradation was conducted as described above.

Phage competition assay

The procedure for carrying out the mutant phage fitness assay was previously reported[23]. To assess the fitness of mutant phages with other phages, 50 µl of wild-type phage (4.5×10^7 p.f.u.s ml^{-1}) was mixed with 50 µl of PaoP5Δ*dap1* (4.5×10^7 p.f.u.s ml^{-1}) and co-cultured with 3 ml of PAO1 (1.5×10^8 c.f.u.s ml^{-1}) for 6 h. Following a 1 min 10,000 × *g* centrifugation to pellet the bacteria from the phage lysates, the phage was transferred to a new tube supplemented with fresh bacterial culture at an MOI of 0.01 (second cycle of competition). Six transfers were performed. Next, using a plaque assay to quantify the relative abundance of PaoP5Δ*dap1* and WT phage in each transfer, 100 plaques were counted for each experiment, with small plaques being classified as PaoP5Δ*dap1* and large plaques as WT phages.

Phylogenetic analysis

The 785 *Pseudomonas* phage genomes were obtained from the NCBI in September 2023. The *dap1*-like genes and *hnh* homologous between the 785 *Pseudomonas* phage genomes and the NCBI phage genome database were identified using Blast. The phylogenetic tree was generated using the neighbour-joining method and 1,000 bootstrap replicates in the MEGA 7 programme[67].

Statistical analyses

The statistical analysis employed in this study involved the utilization of the Student's *t*-test to compare data from two distinct groups. A significance level of $P < 0.05$ was adopted to determine statistical significance.

Reporting summary

Further information on research design is available in the Nature Portfolio Reporting Summary linked to this article.

Data availability

The analysed data and raw RNA-seq readings of PAO1 expressing *dap1* were uploaded to the NCBI GEO (PRJNA1020646). The mass spectrometry proteomics data have been deposited to the ProteomeXchange Consortium (http://proteomecentral.proteomexchange.org) via the iProX[68] partner repository with the dataset identifier PXD046148. The databases used in this study include *P. aeruginosa* PAO1 genome (NC_002516.2), *P. aeruginosa* PA14 genome (NC_008463.1), *P. aeruginosa* phage PaoP5 genome (NC_029083.1), *P. aeruginosa* phage PaP_se genome (OL441337.1), *P. aeruginosa* phage JG004 (NC_019450.1) and *P. aeruginosa* phage PaP8 genome(OL754588.1). Source data are provided with this paper.

References

1. Smith, W. P. J., Wucher, B. R., Nadell, C. D. & Foster, K. R. Bacterial defences: mechanisms, evolution and antimicrobial resistance. *Nat. Rev. Microbiol.* **21**, 519–534 (2023).
2. Bernheim, A. & Sorek, R. The pan-immune system of bacteria: antiviral defence as a community resource. *Nat. Rev. Microbiol.* **18**, 113–119 (2020).
3. Hsueh, B. Y. et al. Phage defence by deaminase-mediated depletion of deoxynucleotides in bacteria. *Nat. Microbiol.* **7**, 1210–1220 (2022).
4. Tock, M. R. & Dryden, D. T. The biology of restriction and anti-restriction. *Curr. Opin. Microbiol.* **8**, 466–472 (2005).
5. Samson, J. E., Magadán, A. H., Sabri, M. & Moineau, S. Revenge of the phages: defeating bacterial defences. *Nat. Rev. Microbiol.* **11**, 675–687 (2013).
6. Huiting, E. et al. Bacteriophages inhibit and evade cGAS-like immune function in bacteria. *Cell* **186**, 864–876.e21 (2023).
7. Davidson, A. R. et al. Anti-CRISPRs: protein inhibitors of CRISPR-Cas systems. *Annu. Rev. Biochem.* **89**, 309–332 (2020).
8. Rifat, D., Wright, N. T., Varney, K. M., Weber, D. J. & Black, L. W. Restriction endonuclease inhibitor IPI* of bacteriophage T4: a novel structure for a dedicated target. *J. Mol. Biol.* **375**, 720–734 (2008).
9. Tesson, F. et al. Systematic and quantitative view of the antiviral arsenal of prokaryotes. *Nat. Commun.* **13**, 2561 (2022).
10. Georjon, H. & Bernheim, A. The highly diverse antiphage defence systems of bacteria. *Nat. Rev. Microbiol.* **21**, 686–700 (2023).
11. Boyle, T. A. & Hatoum-Aslan, A. Recurring and emerging themes in prokaryotic innate immunity. *Curr. Opin. Microbiol.* **73**, 102324 (2023).
12. Goldfarb, T. et al. BREX is a novel phage resistance system widespread in microbial genomes. *EMBO J.* **34**, 169–183 (2015).
13. Shen, B. W. et al. Structure, substrate binding and activity of a unique AAA+ protein: the BrxL phage restriction factor. *Nucleic Acids Res.* **51**, 3513–3528 (2023).
14. Liu, X. et al. Target RNA activates the protease activity of Craspase to confer antiviral defense. *Mol. Cell* **82**, 4503–4518.e8 (2022).
15. Rouillon, C. et al. Antiviral signalling by a cyclic nucleotide activated CRISPR protease. *Nature* **614**, 168–174 (2023).
16. Johnson, A. G. et al. Bacterial gasdermins reveal an ancient mechanism of cell death. *Science* **375**, 221–225 (2022).
17. Roucourt, B. & Lavigne, R. The role of interactions between phage and bacterial proteins within the infected cell: a diverse and puzzling interactome. *Environ. Microbiol.* **11**, 2789–2805 (2009).
18. Wan, X., Hendrix, H., Skurnik, M. & Lavigne, R. Phage-based target discovery and its exploitation towards novel antibacterial molecules. *Curr. Opin. Microbiol.* **68**, 1–7 (2021).
19. Zhang, P. et al. Bacteriophage protein Gp46 is a cross-species inhibitor of nucleoid-associated HU proteins. *Proc. Natl Acad. Sci. USA* **119**, e2116278119 (2022).
20. Liu, J. et al. Antimicrobial drug discovery through bacteriophage genomics. *Nat. Biotechnol.* **22**, 185–191 (2004).

21. Dion, M. B., Oechslin, F. & Moineau, S. Phage diversity, genomics and phylogeny. *Nat. Rev. Microbiol.* **18**, 125–138 (2020).

22. Miller, E. S. et al. Bacteriophage T4 genome. *Microbiol. Mol. Biol. Rev.* **67**, 86–156 (2003).

23. Yuan, S., Shi, J., Jiang, J. & Ma, Y. Genome-scale top-down strategy to generate viable genome-reduced phages. *Nucleic Acids Res.* **50**, 13183–13197 (2022).

24. Repoila, F., Tétart, F., Bouet, J. Y. & Krisch, H. M. Genomic polymorphism in the T-even bacteriophages. *EMBO J.* **13**, 4181–4192 (1994).

25. Shen, M. et al. Characterization and comparative genomic analyses of *Pseudomonas aeruginosa* phage PaoP5: new members assigned to PAK_P1-like viruses. *Sci. Rep.* **6**, 34067 (2016).

26. Hendrix, H. et al. Metabolic reprogramming of *Pseudomonas aeruginosa* by phage-based quorum sensing modulation. *Cell Rep.* **38**, 110372 (2022).

27. Tsao, Y. F. et al. Phage morons play an important role in *Pseudomonas aeruginosa* phenotypes. *J. Bacteriol.* https://doi.org/10.1128/jb.00189-18 (2018).

28. Shah, M. et al. A phage-encoded anti-activator inhibits quorum sensing in *Pseudomonas aeruginosa*. *Mol. Cell* **81**, 571–583.e6 (2021).

29. Chen, G. et al. Structural basis for diguanylate cyclase activation by its binding partner in *Pseudomonas aeruginosa*. *eLife* **10**, e67289 (2021).

30. Kuchma, S. L. et al. BifA, a cyclic-Di-GMP phosphodiesterase, inversely regulates biofilm formation and swarming motility by *Pseudomonas aeruginosa* PA14. *J. Bacteriol.* **189**, 8165–8178 (2007).

31. Xin, L. et al. Regulation of flagellar motor switching by c-di-GMP phosphodiesterases in *Pseudomonas aeruginosa*. *J. Biol. Chem.* **294**, 13789–13799 (2019).

32. Kong, W. et al. ChIP-seq reveals the global regulator AlgR mediating cyclic di-GMP synthesis in *Pseudomonas aeruginosa*. *Nucleic Acids Res.* **43**, 8268–8282 (2015).

33. Chen, L. et al. Characterization and genomic analysis of ValSw3-3, a new Siphoviridae bacteriophage infecting *Vibrio alginolyticus*. *J. Virol.* **94**, e00066-20 (2020).

34. Kala, S. et al. HNH proteins are a widespread component of phage DNA packaging machines. *Proc. Natl Acad. Sci. USA* **111**, 6022–6027 (2014).

35. Leffers, G. G. Jr. & Gottesman, S. Lambda Xis degradation in vivo by Lon and FtsH. *J. Bacteriol.* **180**, 1573–1577 (1998).

36. Yang, N. et al. The Crc protein participates in down-regulation of the Lon gene to promote rhamnolipid production and rhl quorum sensing in *Pseudomonas aeruginosa*. *Mol. Microbiol.* **96**, 526–547 (2015).

37. Herbst, K. et al. Intrinsic thermal sensing controls proteolysis of *Yersinia* virulence regulator RovA. *PLoS Pathog.* **5**, e1000435 (2009).

38. Skorupski, K., Tomaschewski, J., Rüger, W. & Simon, L. D. A bacteriophage T4 gene which functions to inhibit *Escherichia coli* Lon protease. *J. Bacteriol.* **170**, 3016–3024 (1988).

39. Mulvenna, N. et al. Xenogeneic modulation of the ClpCP protease of *Bacillus subtilis* by a phage-encoded adaptor-like protein. *J. Biol. Chem.* **294**, 17501–17511 (2019).

40. Dhungana, G., Nepal, R., Regmi, M. & Malla, R. Pharmacokinetics and pharmacodynamics of a novel virulent *Klebsiella* phage Kp_Pokalde_002 in a mouse model. *Front. Cell. Infect. Microbiol.* **11**, 684704 (2021).

41. Girmenia, C. et al. Incidence, risk factors and outcome of pre-engraftment Gram-negative bacteremia after allogeneic and autologous hematopoietic stem cell transplantation: an Italian prospective multicenter survey. *Clin. Infect. Dis.* **65**, 1884–1896 (2017).

42. Klastersky, J., et al. Bacteraemia in febrile neutropenic cancer patients. *Int. J. Antimicrob.* **30**, S51–S59 (2007).

43. Zhang, K. et al. Bacteriophage protein PEIP is a potent *Bacillus subtilis* enolase inhibitor. *Cell Rep.* **40**, 111026 (2022).

44. Mühlen, S. & Dersch, P. Anti-virulence strategies to target bacterial infections. *Curr. Top. Microbiol. Immunol.* **398**, 147–183 (2016).

45. Rasko, D. A. & Sperandio, V. Anti-virulence strategies to combat bacteria-mediated disease. *Nat. Rev. Drug Discov.* **9**, 117–128 (2010).

46. De Smet, J. et al. Bacteriophage-mediated interference of the c-di-GMP signalling pathway in *Pseudomonas aeruginosa*. *Microb. Biotechnol.* **14**, 967–978 (2021).

47. Ping, D. et al. Hitchhiking, collapse, and contingency in phage infections of migrating bacterial populations. *ISME J.* **14**, 2007–2018 (2020).

48. Hengge, R. Trigger phosphodiesterases as a novel class of c-di-GMP effector proteins. *Phil. Trans. R. Soc. Lond. B* **371**, 20150498 (2016).

49. Rostøl, J. T. & Marraffini, L. (Ph)ighting phages: how bacteria resist their parasites. *Cell Host Microbe* **25**, 184–194 (2019).

50. Uyttebroek, S. et al. Safety and efficacy of phage therapy in difficult-to-treat infections: a systematic review. *Lancet Infect. Dis.* **22**, e208–e220 (2022).

51. Bao, J. et al. Non-active antibiotic and bacteriophage synergism to successfully treat recurrent urinary tract infection caused by extensively drug-resistant *Klebsiella pneumoniae*. *Emerg. Microbes Infect.* **9**, 771–774 (2020).

52. El Ghali, A. et al. Ciprofloxacin in combination with bacteriophage cocktails against multi-drug resistant *Pseudomonas aeruginosa* in ex vivo simulated endocardial vegetation models. *Antimicrob. Agents Chemother.* **67**, e0072823 (2023).

53. Holger, D. J. et al. Phage–antibiotic combinations against multidrug-resistant *Pseudomonas aeruginosa* in in vitro static and dynamic biofilm models. *Antimicrob. Agents Chemother.* **67**, e0057823 (2023).

54. Li, L. et al. First-in-human application of double-stranded RNA bacteriophage in the treatment of pulmonary *Pseudomonas aeruginosa* infection. *Microb. Biotechnol.* **16**, 862–867 (2023).

55. Yang, Y. et al. Development of a bacteriophage cocktail to constrain the emergence of phage-resistant *Pseudomonas aeruginosa*. *Front. Microbiol.* **11**, 327 (2020).

56. Yang, Y. et al. Characterization of the first double-stranded RNA bacteriophage infecting *Pseudomonas aeruginosa*. *Sci. Rep.* **6**, 38795 (2016).

57. Cui, G. et al. PmiR senses 2-methylisocitrate levels to regulate bacterial virulence in *Pseudomonas aeruginosa*. *Sci. Adv.* **8**, eadd4220 (2022).

58. Chua, S. L. et al. Selective labelling and eradication of antibiotic-tolerant bacterial populations in *Pseudomonas aeruginosa* biofilms. *Nat. Commun.* **7**, 10750 (2016).

59. Shen, M. et al. A linear plasmid-like prophage of *Actinomyces odontolyticus* promotes biofilm assembly. *Appl. Environ. Microbiol.* **84**, e01263-18 (2018).

60. Love, M. I., Huber, W. & Anders, S. Moderated estimation of fold change and dispersion for RNA-seq data with DESeq2. *Genome Biol.* **15**, 550 (2014).

61. Zhong, Q. et al. Transcriptomic analysis reveals the dependency of *Pseudomonas aeruginosa* genes for double-stranded RNA bacteriophage phiYY infection cycle. *iScience* **23**, 101437 (2020).

62. Jones, C. J. et al. ChIP-seq and RNA-seq reveal an AmrZ-mediated mechanism for cyclic di-GMP synthesis and biofilm development by *Pseudomonas aeruginosa*. *PLoS Pathog.* **10**, e1003984 (2014).

63. Hickman, J. W. & Harwood, C. S. Identification of FleQ from *Pseudomonas aeruginosa* as a c-di-GMP-responsive transcription factor. *Mol. Microbiol.* **69**, 376–389 (2008).

64. Yang, L. et al. Temperature-dependent carrier state mediated by H-NS promotes the long-term coexistence of *Y. pestis* and a phage in soil. *PLoS Pathog.* **19**, e1011470 (2023).

65. Cen, L. et al. Exploitation of a bacterium-encoded lytic transglycosylase by a human oral lytic phage to facilitate infection. *J. Virol.* **96**, e0106322 (2022).

66. Cai, X. et al. Cultivation of a lytic double-stranded RNA bacteriophage infecting *Microvirgula aerodenitrificans* reveals a mutualistic parasitic lifestyle. *J. Virol.* **95**, e0039921 (2021).

67. Kumar, S., Stecher, G. & Tamura, K. MEGA7: molecular evolutionary genetics analysis version 7.0 for bigger datasets. *Mol. Biol. Evol.* **33**, 1870–1874 (2016).

68. Chen, T. et al. iProX in 2021: connecting proteomics data sharing with big data. *Nucleic Acids Res.* **50**, D1522–d1527 (2022).

Acknowledgements

Author contributions

H.L. and S. Le conceptualized the project. L.W., J.W., F.T., Q.Y. and Z.Z. developed the methodology. H.L. and S. Le performed validation. S. Le, L.W., J.W., F.T., Q.Y., J.Z., Z.Z., J.L. and Q.Z. conducted investigations. H.L., S. Lu and S. Le curated data. X.H., H.L. and S. Le reviewed and edited the manuscript.

Competing interests

The authors declare no competing interests.

Additional information

Extended data is available for this paper at https://doi.org/10.1038/s41564-024-01719-5.

Supplementary information The online version contains supplementary material available at https://doi.org/10.1038/s41564-024-01719-5.

Correspondence and requests for materials should be addressed to Haihua Liang.

Peer review information *Nature Microbiology* thanks Dana Holger, Joshua Ramsay and the other, anonymous, reviewer(s) for their contribution to the peer review of this work. Peer reviewer reports are available.

Reprints and permissions information is available at www.nature.com/reprints.
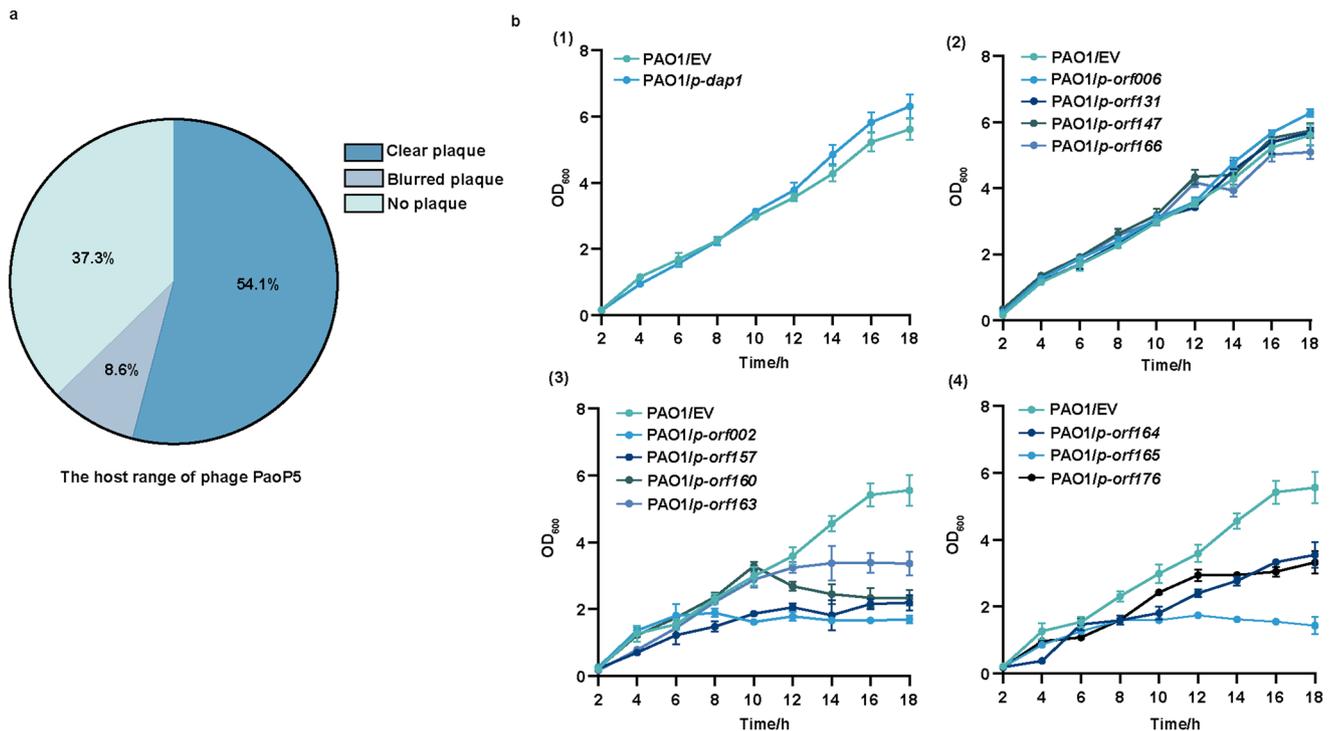
Extended Data Fig. 1 | The host range of PaoP5 and the growth curve of the constructed strains that were determined in LB medium in the presence of 0.05 mM IPTG. (**a**) PaoP5 efficiently lyses 54.1% of the 233 clinically isolated *P. aeruginosa* strains. (**b**) The biological activities of 60 hypothetical *orfs* from PaoP5 were investigated by expressing them individually from pME6032, a multicopy plasmid that could express the target gene when induced by IPTG. The growth of each constructed strain was monitored in LB medium supplemented with 0.05 mM IPTG in the 96-well plates. The OD_{600} was measured for each well using a Microplate Spectrophotometer every 2 h for 18 h. Expression of *orf002, orf157, orf160, orf163, orf164, orf165,* or *orf176* in *P. aeruginosa* attenuated bacterial growth but *orf003 (dap1), orf006, orf131, orf147,* and *orf166* did not. No significant difference was detected between the growth curve of the PAO1 and PAO1/*p-dap1* according to the Two-way Repeated Measures ANOVA analysis (P = 0.115). Error bars indicate the means ± SD of three independent experiments.
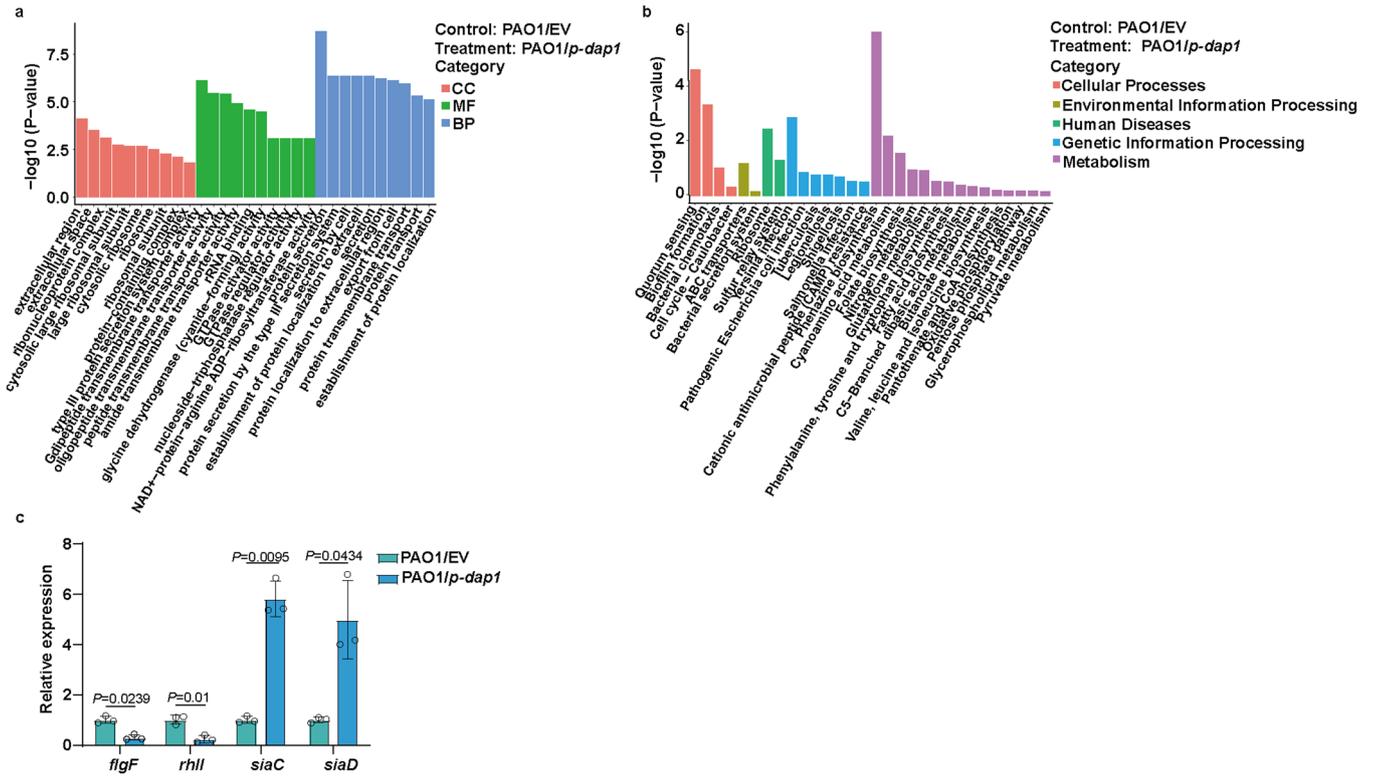
Extended Data Fig. 2 | RNA-seq analysis between PAO1 and PAO1/p-*dap1*.
(**a**) The GO enrichment of the differentially expressed genes in PAO1/EV and
PAO1/p-*dap1* strains, which is classified according to molecular function (MF),
biological process (BP), and cellular component (CC), and the top 10 enriched
GO was shown. *P* values were assessed by two-sided Fisher's exact test and
were adjusted for multiple hypothesis testing using the Benjamini–Hochberg
correction; genes with *p*-values under a threshold of 0.05 were considered
statistically significant. (**b**) The DEGs are classified based on the KEGG analysis,
and the top 30 enriched pathways, including Quorum Sensing and biofilm
formation, are displayed. (**c**) qRT-qPCR analysis of the indicated genes in PAO1/
EV and PAO1/p-*dap1* strains. Data represent mean ± s.d. (n = 3). Statistical
significance was determined using a two-sided Student's *t*-test.
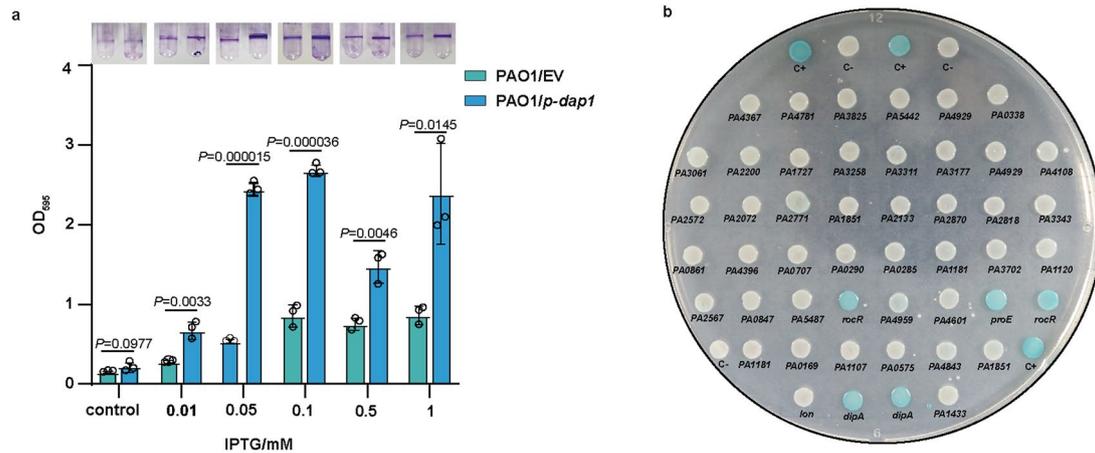
Extended Data Fig. 3 | Impact of *dap1* on biofilm formation and the bacterial two-hybrid results of Dap1 with 42 proteins. (**a**) The biofilm formation of PAO1/EV and PAO1/*p-dap1* under LB conditions supplemented with different concentrations of IPTG was displayed with crystal violet staining and quantified with optical density measurement. Data represent mean ± s.d. (n = 3) and statistical significance was determined using a two-sided Student´s *t*-test. (**b**) Bacterial two-hybrid assay determined the interaction between Dap1 with 42 c-di-GMP metabolic enzymes. The pUT18C is fused to Dap1 protein and the pKT25 is fused to the target proteins. Interactions were visualized by a drop test on LB agar plates supplemented with X-gal. The blue colonies showing the interaction between Dap1 and the indicated proteins. Strains containing the pKT25 and pUT18 vectors were used as a negative control (C-), and the interaction between *pUT18C-zip* and *pKT25-zip* was used as a positive control (C+).
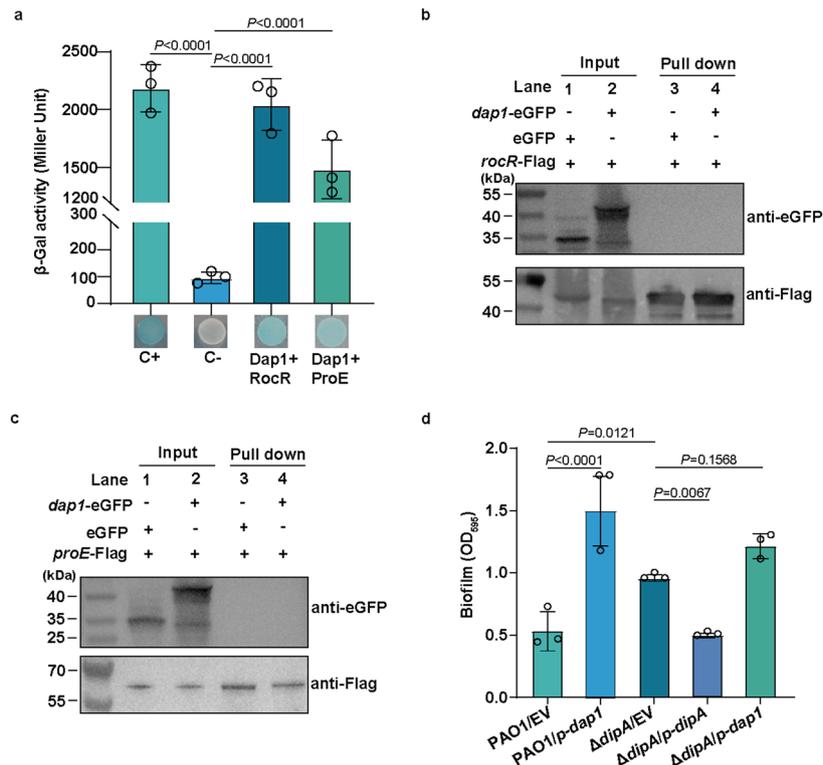
Extended Data Fig. 4 | Interactions of Dap1 with other proteins. (a) The bacterial two-hybrid assay indicated that Dap1 might interact with RocR and ProE. Interactions were visualized by a drop test on LB agar plates supplemented with X-gal, and quantified by measuring the β-galactosidase activity indicated in Miller Units. **(b-c)** Co-IP assays showing no interaction between Dap1 with either RocR **(b)** or ProE **(c)** Overnight cultures of *E. coli* harboring *rocR-Flag* (or *proE-Flag*) with either eGFP or *dap1*-eGFP were lysed. Cell-lysis supernatants were incubated with anti-Flag beads, and then proteins were detected by western blot with eGFP or Flag antibody. Each experiment was repeated three times independently with similar results. **(d)** The biofilm formation of the indicated strains was displayed with crystal violet staining and quantified with optical density measurement. Data in a and d represent mean ± s.d. (n = 3) and statistical significance was determined using a one-way ANOVA Dunnett's multiple comparison test.
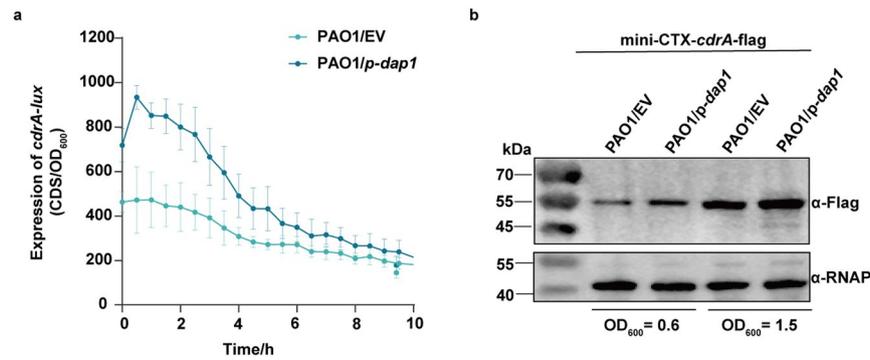
Extended Data Fig. 5 | Expression of *dap1* in PAO1 increased the transcript and protein level of CdrA. (**a**) Strains harboring the *cdrA-lux* and *p-dap1* plasmids were cultivated in LB medium supplemented with 0.05 mM IPTG. The promoter activity of *cdrA* was detected at the indicated time. Error bars indicated the mean ± s.d. of three biological replicates. (**b**) CdrA protein levels were measured in PAO1/EV and PAO1/*p-dap1* strains. Bacteria were cultured to an OD_{600} of 0.6 and 1.5. Equivalent samples were loaded onto SDS-PAGE and detected with an anti-Flag antibody. α-RNA polymerase (RNAP) was used as a loading control.

a

b

PaoP5Δ*dap1* + PAO1 PaoP5Δ*dap1* + Δ*dipA*
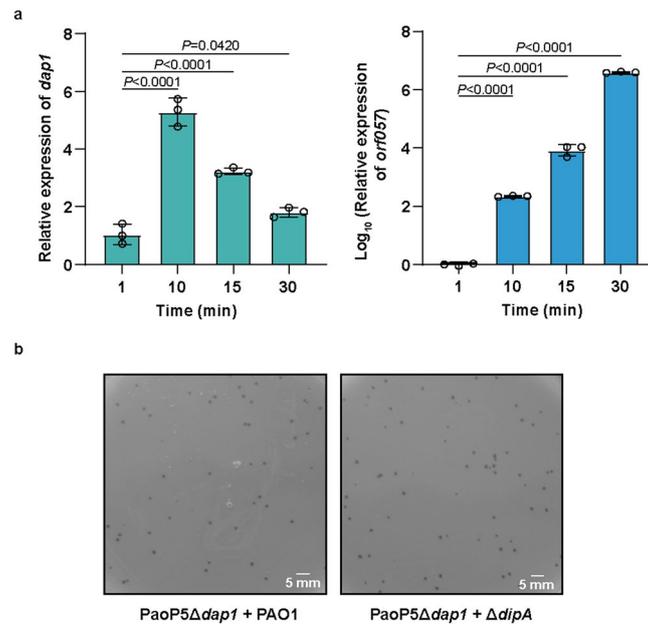
Extended Data Fig. 6 | DipA is an early expressed gene and deletion of *dipA* had no effect on phage plaque formation. (**a**) RT-qPCR analysis of *dap1 and orf57* at 1 min, 10 min, 15 min and 30 min after phage infection. The highest level of dap1 transcript was detected 10 mins after phage infection, while the mRNA of the structural protein Orf57 was highly expressed 30 min after phage infection.

(**b**) The same number of phage PaoP5Δ*dap1* was mixed with PAO1 or Δ*dipA*, and used double-layer agar plates to observe the plaque number and size. Data in a-b represent mean ± s.d. (n = 3) and statistical significance was determined using a one-way ANOVA Dunnett's multiple comparison test.
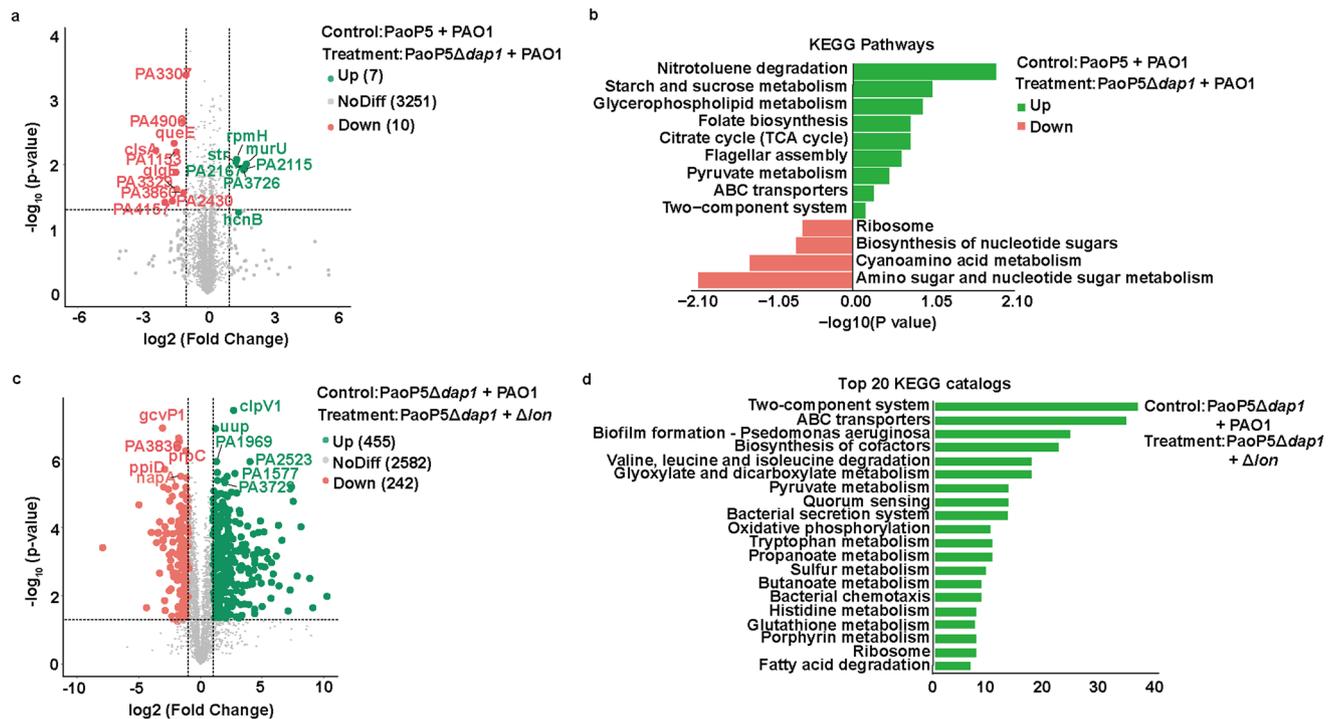
Extended Data Fig. 7 | The differentially expressed proteins detected by proteomics analysis. (**a**) The differentially expressed bacterial proteins (DEPs) of PaoP5 or PaoP5Δ*dap1* infected PAO1. Only 17 bacterial proteins were significantly changed during PaoP5 and PaoP5Δ*dap1* infection, including seven upregulated proteins and ten downregulated proteins. (**b**) Showing the KEGG enrichments of these DEPs between PaoP5 or PaoP5Δ*dap1*. (**c**) The DEPs of PaoP5Δ*dap1* infected PAO1 and Δ*lon*. *P* values were assessed by two-sided Fisher's exact test and were adjusted for multiple hypothesis testing using the Benjamini–Hochberg correction, proteins with *p*-values under a threshold of 0.05 were considered as statistically significant. (**d**) The DEPs between PaoP5Δ*dap1* infected PAO1 and Δ*lon* were classified according to the KEGG enrichment, and the top 20 KEGG catalogs, including two-component system, ABC transporters, and biofilm formation are displayed.

PaoP5 + PAO1   PaoP5Δ*dap1* + PAO1

PaoP5Δ*dap1* + PAO1/*p-dap1*   PaoP5Δ*dap1* + PAO1/*p-orf050*

PaoP5Δ*dap1* + Δ*lon*   PaoP5Δ*dap1* + Δ*lon*/*p-lon*
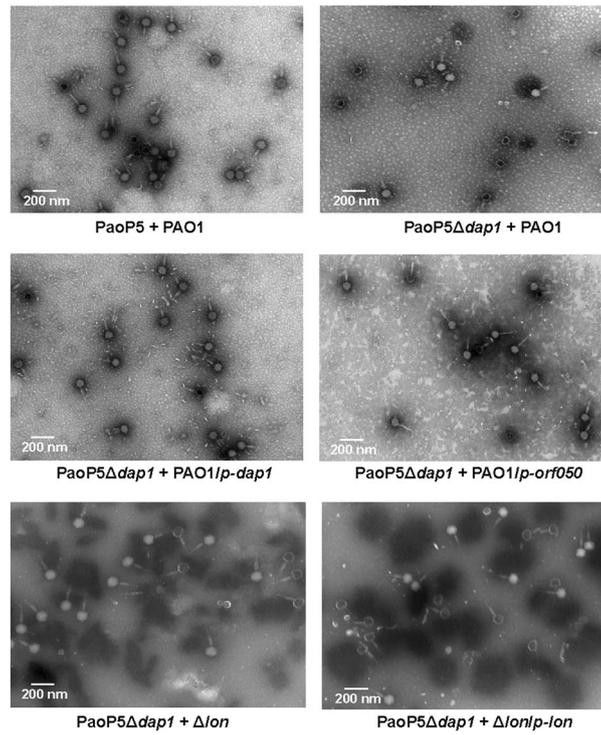
Extended Data Fig. 8 | Representative transmission electron micrographs of phages. Representative transmission electron micrographs of negatively stained phages produced in PAO1, PAO1/*p-dap1*, Δ*lon*, and Δ*lon*/*p-lon*. The empty capsids are black, and phages with white heads are packaged with the genomes. Each experiment was repeated three times independently with similar results.
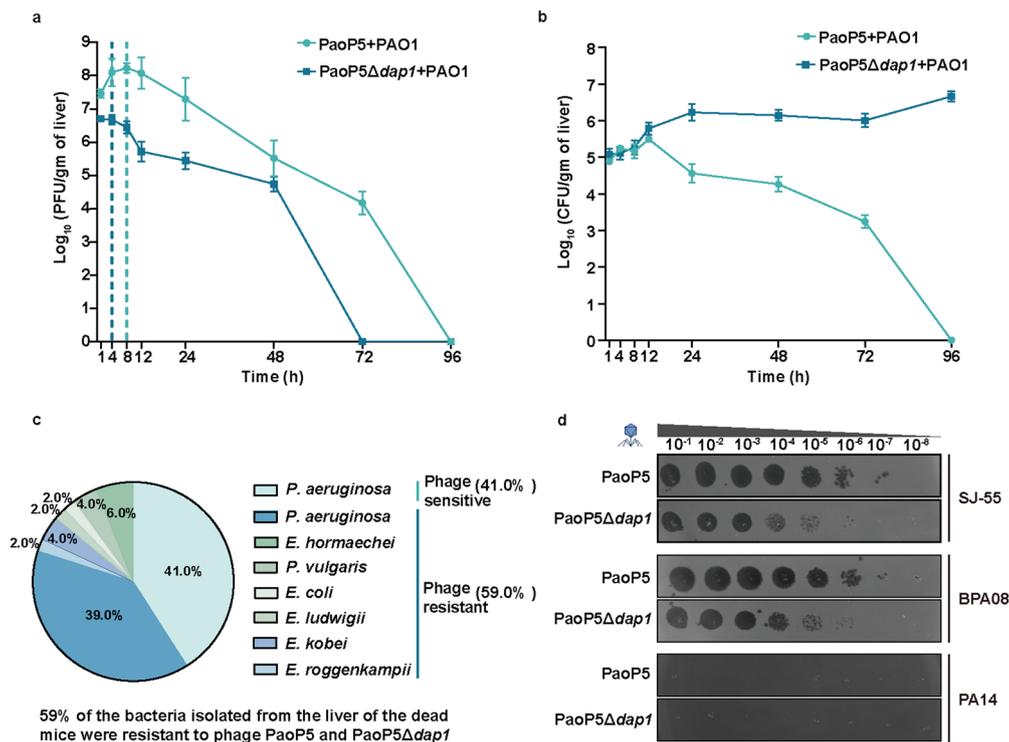
Extended Data Fig. 9 | The phage and bacterial counts in the liver of the mice.
Phage titer (**a**) and the bacterial CFU (**b**) detected in the liver of mice that were
intraperitoneal injected with PAO1 and phage PaoP5Δ*dap1* or PaoP5 at an MOI of
10. The maximum titer of PaoP5 was detected at 8 h post phage injection (~1.75
× 10^8 PFU/gm). The phage titer gradually decreased after 24 h, and was cleared
within 96 h. Meanwhile, the bacterial CFU in the liver decreased gradually and
was cleared within 96 h. For the PaoP5Δ*dap1*- treated, PAO1-infected mice, the
phage titer continuously decreased to an undetectable level at 72 h, and the
maximum titer of PaoP5Δ*dap1* in the liver (~5 × 10^6 PFU/gm) was much less than
that of PaoP5-treated mice. a-b, Error bars indicated the mean ± s.d. (n = 4 mice).
(**c**) Classification of the bacteria detected in the liver of the dead mice that were

treated with PaoP5Δdap1. 4 mice that were dead 48 h after phage PaoP5Δdap1
therapy were selected, and 50 colonies were isolated from the liver of each mouse
and 200 colonies were assessed for phage resistance. 82 colonies were phage
sensitive, and 118 colonies were phage resistant to both PaoP5 and PaoP5Δdap1.
30 phage-resistant strains were sent for 16 s rDNA sequencing. Overall, 41% of
these strains were phage-sensitive *P. aeruginosa*, 39% of the strains were phage-
resistant *P. aeruginosa*, while the other phage-resistant strains are gut commensal
bacteria, including *Enterobacter hormaechei*, *Proteus vulgaris*, *Escherichia coli*,
Enterobacter ludwigii, *Enterobacter kobei* and *Enterobacter roggenkampii*. (**d**)
PaoP5 forms large plaques on some clinical strains while PaoP5Δdap1 forms small
plaques, but both phages could not infect PA14.
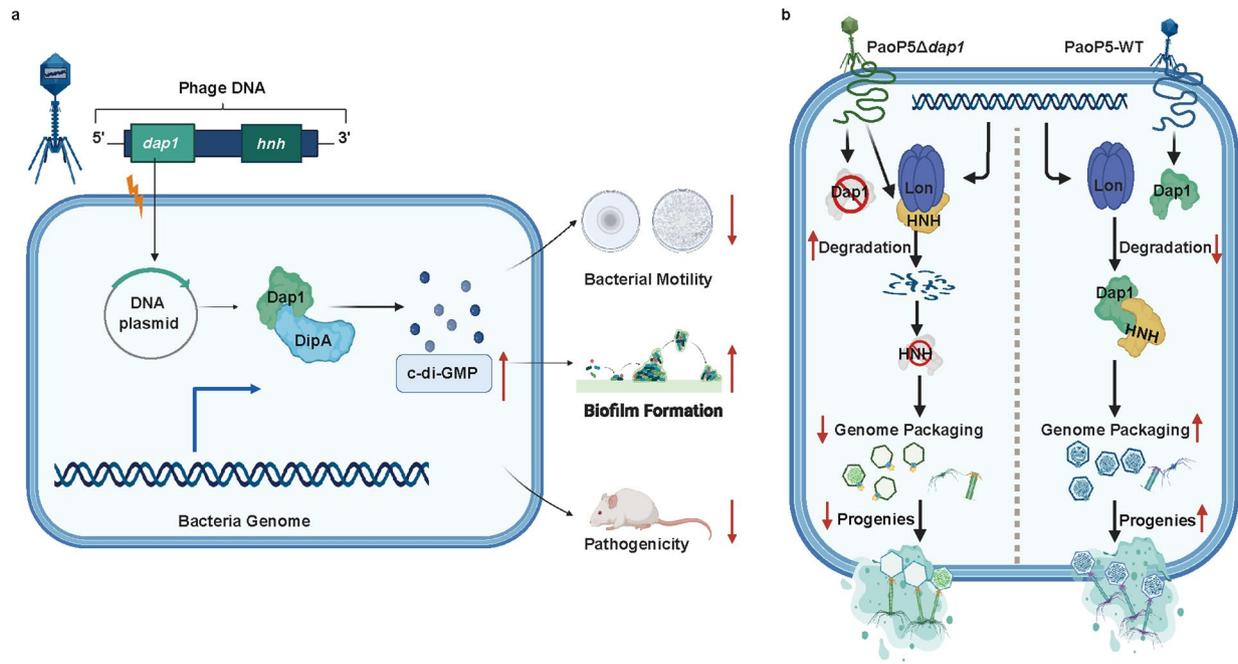
Extended Data Fig. 10 | Model of the mechanisms by which Dap1 regulates bacterial virulence and evades the Lon-mediated anti-phage defense.
(**a**) Phage protein Dap1 interacting with DipA leads to an increase in the cellular c-di-GMP levels, which inhibits bacterial motility, promotes biofilm formation, and significantly attenuates the virulence of *P. aeruginosa*. (**b**) When PaoP5 infects PAO1, phage protein Dap1 binds to HNH endonuclease to evade Lon-mediated HNH degradation; thus, more progenies are packaged with genomic DNA. However, the HNH endonuclease is efficiently degraded by Lon in the absence of Dap1, which facilitates PaoP5Δ*dap1* to produce fewer progenies, and most capsids are empty.PA14.

nature portfolio

Corresponding author(s): Haihua Liang

Last updated by author(s): Apr 5, 2024

Reporting Summary

Nature Portfolio wishes to improve the reproducibility of the work that we publish. This form provides structure for consistency and transparency in reporting. For further information on Nature Portfolio policies, see our Editorial Policies and the Editorial Policy Checklist.

Statistics

For all statistical analyses, confirm that the following items are present in the figure legend, table legend, main text, or Methods section.

n/a	Confirmed	
☐	☒	The exact sample size (*n*) for each experimental group/condition, given as a discrete number and unit of measurement
☐	☒	A statement on whether measurements were taken from distinct samples or whether the same sample was measured repeatedly
☐	☒	The statistical test(s) used AND whether they are one- or two-sided *Only common tests should be described solely by name; describe more complex techniques in the Methods section.*
☒	☐	A description of all covariates tested
☐	☒	A description of any assumptions or corrections, such as tests of normality and adjustment for multiple comparisons
☐	☒	A full description of the statistical parameters including central tendency (e.g. means) or other basic estimates (e.g. regression coefficient) AND variation (e.g. standard deviation) or associated estimates of uncertainty (e.g. confidence intervals)
☐	☒	For null hypothesis testing, the test statistic (e.g. *F*, *t*, *r*) with confidence intervals, effect sizes, degrees of freedom and *P* value noted *Give P values as exact values whenever suitable.*
☒	☐	For Bayesian analysis, information on the choice of priors and Markov chain Monte Carlo settings
☒	☐	For hierarchical and complex designs, identification of the appropriate level for tests and full reporting of outcomes
☒	☐	Estimates of effect sizes (e.g. Cohen's *d*, Pearson's *r*), indicating how they were calculated

Our web collection on statistics for biologists contains articles on many of the points above.

Software and code

Policy information about availability of computer code

Data collection | Proteomic data were analyzed by LC-MS/MS, the protein sequences of differentially expressed proteins were retrieved using NCBI BLAST+ client software and compared with the online Kyoto Encyclopedia of Genes and Genomes(KEGG) database; RNA-seq reads were mapped to the P.aeruginosa genomes provided by National Center for Biotechnology Indormation using Bowtie2, and only the uniquely mapped reads were kept for the subsequent analyses; The data of the evolutional tree comes from NCBI and analysis by MEGA7.

Data analysis | NCBI blast+ 2.15.0; Graphpad Prism 8.0.2; MEGA 7.0.21; Bowtie2 (2.5.1); Htseq 0.9.1; Deseq 1.38.3; clusterprofiler 4.6.0.

For manuscripts utilizing custom algorithms or software that are central to the research but not yet described in published literature, software must be made available to editors and reviewers. We strongly encourage code deposition in a community repository (e.g. GitHub). See the Nature Portfolio guidelines for submitting code & software for further information.

Data

Policy information about availability of data

All manuscripts must include a data availability statement. This statement should provide the following information, where applicable:
- Accession codes, unique identifiers, or web links for publicly available datasets
- A description of any restrictions on data availability
- For clinical datasets or third party data, please ensure that the statement adheres to our policy

The data are available in the manuscript, supplementary materials and raw dataset. Inaddition, small and total RNA sequencing data are available on the NCBI

Research involving human participants, their data, or biological material

Policy information about studies with [human participants or human data](). See also policy information about [sex, gender (identity/presentation), and sexual orientation]() and [race, ethnicity and racism]().

Reporting on sex and gender	N/A
Reporting on race, ethnicity, or other socially relevant groupings	N/A
Population characteristics	N/A
Recruitment	N/A
Ethics oversight	N/A

Note that full information on the approval of the study protocol must also be provided in the manuscript.

Field-specific reporting

Please select the one below that is the best fit for your research. If you are not sure, read the appropriate sections before making your selection.

☒ Life sciences ☐ Behavioural & social sciences ☐ Ecological, evolutionary & environmental sciences

For a reference copy of the document with all sections, see nature.com/documents/nr-reporting-summary-flat.pdf

Life sciences study design

All studies must disclose on these points even when the disclosure is negative.

Sample size	The sample size is determined following the strandrad experimental designs in this field, without pre-calculation of the sample size. Experiments were performed in at least 3 independent replicates, which is sufficient to avoid random variations.
Data exclusions	No data was excluded.
Replication	All experiments were performed with three biological replicates.
Randomization	Bacteria samples was not randomised since we employed well-defined experimental strain with isogenic genetic backgrounds, comparing effects of single, known variables. Animals were allocated randomly to experimental groups.
Blinding	Blinding was not relevant to this study, since no manual counting or scoring was performed to obtain data.

Behavioural & social sciences study design

All studies must disclose on these points even when the disclosure is negative.

Study description	
Research sample	
Sampling strategy	
Data collection	
Timing	
Data exclusions	
Non-participation	

Randomization | |

Ecological, evolutionary & environmental sciences study design

All studies must disclose on these points even when the disclosure is negative.

Study description | |

Research sample | |

Sampling strategy | |

Data collection | |

Timing and spatial scale | |

Data exclusions | |

Reproducibility | |

Randomization | |

Blinding | |

Did the study involve field work? ☐ Yes ☐ No

Field work, collection and transport

Field conditions | |

Location | |

Access & import/export | |

Disturbance | |

Reporting for specific materials, systems and methods

We require information from authors about some types of materials, experimental systems and methods used in many studies. Here, indicate whether each material, system or method listed is relevant to your study. If you are not sure if a list item applies to your research, read the appropriate section before selecting a response.

Materials & experimental systems

n/a	Involved in the study
☐	☒ Antibodies
☒	☐ Eukaryotic cell lines
☒	☐ Palaeontology and archaeology
☐	☒ Animals and other organisms
☒	☐ Clinical data
☒	☐ Dual use research of concern
☒	☐ Plants

Methods

n/a	Involved in the study
☒	☐ ChIP-seq
☒	☐ Flow cytometry
☒	☐ MRI-based neuroimaging

Antibodies

Antibodies used | Mouse anti DDDDK-Tag mAb (AE005, Abclonal, 1:1000); Anti-GFP mAb (AE078, Abclonal,1:10000); Mouse anti His-Tag mAb (AE003, Abclonal, 1:5000); HRP Goat Anti-Rabbit IgG (AS014, Abclonal, 1:2000); HRP Goat Anti-Mouse IgG (AS003, Abclonal, 1:2000); Purified anti-E.coli RNA Polymerase α Antibody (663014, Biolegend, 1:5000).

Validation	Antibodies were used according to the validation listed in manufacturer's instructions. The details of antibody validation are given in Supplementary Data Table 1-4.

Eukaryotic cell lines

Policy information about cell lines and Sex and Gender in Research

Cell line source(s)	
Authentication	
Mycoplasma contamination	
Commonly misidentified lines (See ICLAC register)	

Palaeontology and Archaeology

Specimen provenance	
Specimen deposition	
Dating methods	

☐ Tick this box to confirm that the raw and calibrated dates are available in the paper or in Supplementary Information.

Ethics oversight	

Note that full information on the approval of the study protocol must also be provided in the manuscript.

Animals and other research organisms

Policy information about studies involving animals; ARRIVE guidelines recommended for reporting animal research, and Sex and Gender in Research

Laboratory animals	All procedures performed with 7 week-old BALB/c female mice. The mice were purchased from Hunan SJA Laboratory Animal Co., Ltd., and were housed under specific pathogen-free (SPF) conditions, and the housing environment had controlled temperature (20-26 °C), humidity (40-70%) and lighting conditions (12 h light and 12 h dark cycles), and no animal was excluded from the analyses.
Wild animals	The study did not involve wild animals.
Reporting on sex	All female mice were used in this study.
Field-collected samples	No field-collected samples were used.
Ethics oversight	The Animal Research Ethics Committee of Army Medical University reviewed, approved, and supervised the protocols for animal research (permit number: AMUWEC20230178, AMUWEC20230470).

Note that full information on the approval of the study protocol must also be provided in the manuscript.

Clinical data

Policy information about clinical studies
All manuscripts should comply with the ICMJE guidelines for publication of clinical research and a completed CONSORT checklist must be included with all submissions.

Clinical trial registration	
Study protocol	
Data collection	
Outcomes	

Dual use research of concern

Policy information about dual use research of concern

Hazards

Could the accidental, deliberate or reckless misuse of agents or technologies generated in the work, or the application of information presented in the manuscript, pose a threat to:

No | Yes

☐ | ☐ Public health

☐ | ☐ National security

☐ | ☐ Crops and/or livestock

☐ | ☐ Ecosystems

☐ | ☐ Any other significant area

Experiments of concern

Does the work involve any of these experiments of concern:

No | Yes

☐ | ☐ Demonstrate how to render a vaccine ineffective

☐ | ☐ Confer resistance to therapeutically useful antibiotics or antiviral agents

☐ | ☐ Enhance the virulence of a pathogen or render a nonpathogen virulent

☐ | ☐ Increase transmissibility of a pathogen

☐ | ☐ Alter the host range of a pathogen

☐ | ☐ Enable evasion of diagnostic/detection modalities

☐ | ☐ Enable the weaponization of a biological agent or toxin

☐ | ☐ Any other potentially harmful combination of experiments and agents

Plants

Seed stocks | N/A

Novel plant genotypes | N/A

Authentication | N/A

ChIP-seq

Data deposition

☐ Confirm that both raw and final processed data have been deposited in a public database such as GEO.

☐ Confirm that you have deposited or provided access to graph files (e.g. BED files) for the called peaks.

Data access links
May remain private before publication. | N/A

Files in database submission | N/A

Genome browser session
(e.g. UCSC) | N/A

Methodology

Replicates | N/A

Sequencing depth	N/A
Antibodies	N/A
Peak calling parameters	N/A
Data quality	N/A
Software	N/A

Flow Cytometry

Plots

Confirm that:

☐ The axis labels state the marker and fluorochrome used (e.g. CD4-FITC).

☐ The axis scales are clearly visible. Include numbers along axes only for bottom left plot of group (a 'group' is an analysis of identical markers).

☐ All plots are contour plots with outliers or pseudocolor plots.

☐ A numerical value for number of cells or percentage (with statistics) is provided.

Methodology

Sample preparation	
Instrument	
Software	
Cell population abundance	
Gating strategy	

☐ Tick this box to confirm that a figure exemplifying the gating strategy is provided in the Supplementary Information.

Magnetic resonance imaging

Experimental design

Design type	
Design specifications	
Behavioral performance measures	

Acquisition

Imaging type(s)	
Field strength	
Sequence & imaging parameters	
Area of acquisition	

Diffusion MRI ☐ Used ☐ Not used

Preprocessing

Preprocessing software	
Normalization	
Normalization template	

Noise and artifact removal

Volume censoring

Statistical modeling & inference

Model type and settings

Effect(s) tested

Specify type of analysis: ☐ Whole brain ☐ ROI-based ☐ Both

Statistic type for inference

(See <u>Eklund et al. 2016</u>)

Correction

Models & analysis

n/a	Involved in the study
☐	☐ Functional and/or effective connectivity
☐	☒ Graph analysis
☐	☐ Multivariate modeling or predictive analysis

Functional and/or effective connectivity

Graph analysis

Multivariate modeling and predictive analysis